1. Title page

Specific GPCRs Elicit Unique Extracellular Vesicle MiRNA Array Signatures: An Exploratory Study

Xiao Shi, Michelle C. Palumbo, Sheila Benware, Jack Wiedrick, Sheila Markwardt, Aaron Janowsky

Affiliations:

XS, SB, AJ: Research Service, Veterans Affairs Portland Health Care System, Portland OR 97239

MCP, AJ: Department of Behavioral Neuroscience, Oregon Health & Science University, Portland OR 97239 USA

JW, SM: Biostatistics & Design Program, OHSU-PSU School of Public Health, Oregon Health & Science University, Portland OR 97239 USA

AJ: Department of Psychiatry, Oregon Health & Science University, Portland OR 97239 USA

Laboratory of Origin:

Aaron Janowsky, Research Service, Veterans Affairs Portland Health Care System

Oregon Health & Science University, Portland OR 97239 USA

2. Running title page

Running title: Activating GPCRs regulates extracellular vesicle miRNA content

Corresponding author: Xiao Shi, Ph.D.

Address: Research Service, VA Portland Health Care System, 3710 SW US Veterans Hospital Rd., Portland, OR 97239

Telephone: (503) 418-5376

Fax: (503) 721-7839

Email: shixi@ohsu.edu

Number of text page: 36

Number of tables: 1

Number of figures: 4

Number of references: 105

Abstract word count: 225

Introduction word count: 672

Discussion word count: 1779

Nonstandard abbreviations used: ACKR3, atypical chemokine receptor 3; ADORA1, adenosine receptor A1; ANOVA, analysis of variance; CCPA: 2-Chloro-N^6-cyclopentyladenosine; DPCPX, 8-Cyclopentyl-1,3-dipropylxanthine; ERK, extracellular signal-regulated kinase; EV, extracellular vesicle; FZD4, frizzled class receptor 4; GPCR, G protein-coupled receptor; HRH1, histamine receptor H1;

KEGG, Kyoto Encyclopedia of Genes and Genomes; miRNA, microRNA; NTA, nanoparticle tracking analysis; PEA, 2-pyridylethylamine; PPI, protein-protein interaction; qPCR, quantitative polymerase chain reaction; SEC, size exclusion chromatography; SDF-1α, stromal derived factor-1α; TEM, transmission electron microscopy; Wnt3A, Wnt family member 3A.

3. Abstract:

All cells secrete extracellular vesicles (EVs) containing nucleic acid cargo, including microRNAs (miRNAs), that regulate the function of receiving cells. G protein-coupled receptors (GPCRs) affect intracellular function via multiple signaling cascades. However, the mechanisms of GPCR intercellular signaling through EV miRNA activity are unknown. Human U2 osteosarcoma cells expressing native GPCRs were used to selectively stimulate distinct G protein signaling cascades ($G\alpha_i$, $G\alpha_q$, $G\alpha_{12/13}$, and β-arrestin) by members of specific receptor subclasses including the adenosine receptor A1 (ADORA1), the histamine receptor H1 (HRH1), the frizzled class receptor 4 (FZD4), and the atypical chemokine receptor 3 (ACKR3), respectively. We hypothesized that stimulation of specific classes of GPCRs would cause the release of EVs containing miRNAs with receptor-specific up- or down-regulated expression, affecting unique pathological downstream signaling cascades. Receptor-specific agonists dose-dependently increased respective signaling cascade intermediates. We found no change in the quantity of EVs (~200nm diameter), but there were distinct EV miRNA signatures following stimulation of GPCRs. Network analyses of differentially expressed miRNA and their predicted targets validated the linkage between specific receptors and cell function and pathological states. The data can be used to reverse engineer mechanisms involving EV miRNAs for various physiological and pathological processes. GPCRs are major pharmacological targets, so understanding the mechanisms that stimulate or inhibit GPCR-mediated changes in extracellular miRNA signatures could improve long- and short-term therapeutic and unwanted drug effects.

Summary: Stimulation of specific GPCRs elicited unique EV miRNA signatures that up- and down-regulated predicted biological and pathological cellular processes.

Key words

G protein-coupled receptor, receptor signaling, miRNA, extracellular vesicle, U2OS

4. Significance Statement

G protein-coupled receptors (GPCR) are therapeutic targets for various human diseases. However, the mechanisms of GPCR signaling through extracellular vesicle (EV) miRNA activity are unknown. Here, we identified unique EV miRNA signatures resulting from GPCR activation. The miRNA functional analyses indicate that the downstream signaling effects and their functional networks differ by receptor. This study has important implications for developing new drugs and their long-term and "off-target" effects.

5. Visual Abstract

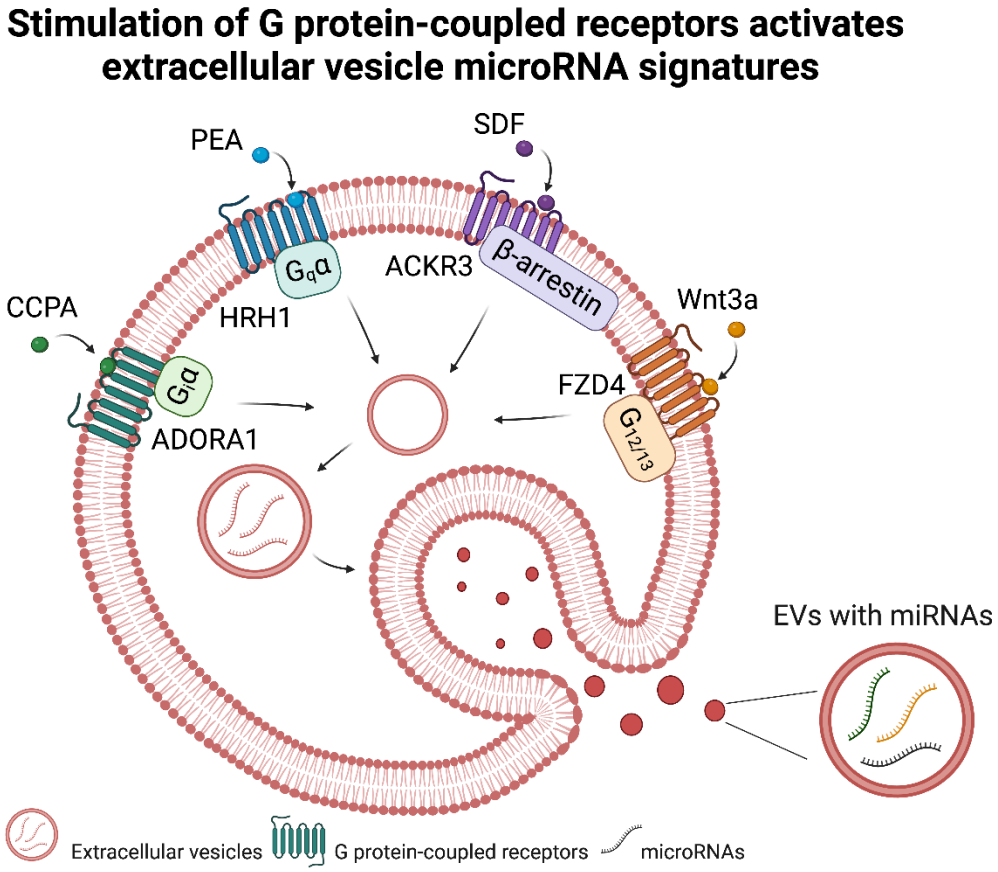

6. INTRODUCTION

G protein-coupled receptors (GPCRs) comprise a protein superfamily with five major branches: glutamate, rhodopsin, adhesion, frizzled/taste 2, and secretin (Stevens et al., 2013). These transmembrane proteins transduce neurotransmitter signals from outside the cell to affect internal cellular function (Stevens et al., 2013). Translation of extracellular signals to intracellular biochemical cascades is a multistep process involving specific receptor-ligand interactions, conformational changes allowing interactions with regulatory G proteins such as, $G\alpha_i$, $G\alpha_q$, $G\alpha_{12/13}$, and β-arrestin, and activation of specific effector systems (Asher et al., 2022; Heydenreich et al., 2023). GPCR function or malfunction is implicated in numerous human diseases, and approximately 700 medications are designed to target GPCRs and related proteins (Sriram & Insel, 2018) and to alter cellular activity. In addition to the canonical intracellular protein cascades, GPCR signaling is both a precursor and effector of extracellular mechanisms of communication (Bebelman et al., 2020).

Cells interact through the secretion and uptake of extracellular vesicles (EVs) (Rothman, 1996). EVs are a heterogeneous population of membrane vesicles that are classified into exosomes, microvesicles, and apoptotic bodies based on their biogenesis, release pathways, size, content, and function (Doyle & Wang, 2019) (Palmisano et al., 2012). EVs transport a range of molecules such as nucleic acids including microRNAs (miRNA), lipids, and proteins associated with the cell lipid membrane such as GPCRs (Kahn et al., 2017; Mack et al., 2000). GPCRs and EVs have interacting functions since EV biogenesis and release can be regulated by GPCR stimulation, and EVs can contribute to GPCR signaling (Kriebel et al., 2018; Frederik Johannes Verweij et al., 2018). In fact, a number of GPCRs alter EV release and/or EV cargo (Bhattacharya et al., 2023; Conrad et al., 2020; Lee et al., 2023). However, the effects of stimulating specific GPCR subclasses, in head-to-head comparisons, on EV content and subsequent alteration of receiving cell function remain to be elucidated (Tetta et al., 2013).

MiRNAs are small non-coding RNAs (Tabara et al., 2002) and play crucial roles in plant and animal physiology, including development (Zhang et al., 2015). They are implicated in symptoms of pathology at the intersection of substance use and HIV (Odegaard et al., 2020), Alzheimer's disease (Sandau et al., 2022), and diabetes (Chao et al., 2023). MiRNAs function by translationally repressing target mRNA transcripts. The human genome includes approximately 2,600 miRNAs, and individual miRNAs can regulate tens to hundreds of gene targets (Plotnikova et al., 2019). Therefore, miRNAs are one of the largest classes of regulatory RNAs that affect complex genetic networks. However, whether GPCRs are post-transcriptionally affected by miRNAs is controversial (Ofer & Linial, 2022; Orr-Burks et al., 2021).

Many drugs that stimulate GPCRs affect EV miRNA disposition. For example, ethanol potentiates GABA-A receptor function and alters EV miRNA expression (Bourgeois et al., 2023). Methamphetamine use alters groups of human plasma EV miRNAs (Sandau et al., 2020). Bombesin receptor subtype 3 stimulation results in its own incorporation into EVs and alteration of RhoA function in receiving cells (Z. Wang et al., 2022). GPCRs affect EV secretion and miRNA expression pertaining to platelet aggregation, function, and activation (Ambrose et al., 2018; Jin et al., 2022). Additionally, stimulation of CXCR7, a chemokine receptor, results in expression changes of specific miRNAs related to colorectal cancer metastasis. However, it is unknown if stimulation of specific GPCR subclasses affects EV miRNA content to alter downstream cellular communication, as well as signal cascades involved in physiology and disease. Using U2OS cells, we examined the effects of stimulating the adenosine receptor A1 (ADORA1), the histamine receptor H1 (HRH1), and atypical chemokine receptor 3 (ACKR3), members of the Rhodopsin-like GPCR family, as well as the frizzled class receptor 4 (FZD4). These receptors are $G\alpha_i$-, $G\alpha_q$-, β-arrestin-, and $G\alpha_{12/13}$-coupled, respectively. Stimulation resulted in the release of EVs with unique miRNA signatures. Network analyses of EV miRNA target transcripts showed both up- and down-regulation of protein cascades involved in physiological and pathological states of cell function. This

work demonstrates the large-scale genetic influence of miRNA arrays as a product of GPCR stimulation and can be used to characterize down-stream pharmacological effects of receptor-drug interactions.

7. RESULTS

GPCR expression in U2OS cells

To characterize the effect of GPCR stimulation on EV miRNA content, we examined GPCR expression in different cell lines from The Human Protein Atlas (Karlsson et al., 2021). We determined that the human osteosarcoma cell line, U2OS, likely expressed receptors from multiple branches of the GPCR family tree (https://www.proteinatlas.org/search/U2OS+cells), including rhodopsin, adhesion, and frizzle/taste receptors, each associated with differing G-protein cascade activation (Supplemental Tab. S1). Numerous other cell lines including U-251MG, A-431 and SH-SY5Y, were considered but not used because they did not highly express a significant spread of receptor subtypes (Supplemental Tab. S1). Additionally, we avoided the use of transfected or over-expressing cells because the transfection and selection protocols could have their own effects on EV synthesis, expression, and cargo selection (Im et al., 2019; Németh et al., 2017; Nordin, 2022). The protein expression data of U2OS cells provided by the Human Protein Atlas database indicated that ADORA1, HRH1, ACKR3, and FZD4 were expressed at levels sufficient to demonstrate second messenger system activity, i.e., function.

The expression of these receptors in U2OS cells was further validated through various functional assays. 2-Chloro-N^6-cyclopentyladenosine (CCPA), an ADORA1 selective agonist, dose-dependently inhibited forskolin-induced cAMP levels (Fig. 1A). The inhibition of cAMP by CCPA was reduced by antagonist 8-Cyclopentyl-1,3-dipropylxanthine (DPCPX), suggesting that the decreased cAMP level resulted from ADORA1 activation. The activation of HRH1 was assessed by measuring inositol monophosphate (IP1) accumulation following 2-pyridylethylamine dihydrochloride (PEA) stimulation, and the effect was

abolished by the HRH1 antagonist cetirizine (Fig. 1B). To evaluate the function of FZD4, we measured the activity of alkaline phosphatase (ALP), the downstream gene product of the Wnt/β-catenin signaling cascade. Norrin, another FZD4 agonist, has high affinity (Xu et al., 2004). However, Norrin is difficult to purify from mammalian sources (Perez-Vilar & Hill, 1997). We found the commercially available Norrin (R&D Systems) did not stimulate FZD4 (data not shown). Although Wnt family member 3A (Wnt3A) can bind to several members of the frizzled receptor family, it has much higher affinity binding at FZD4 than FZD8 (Kozielewicz et al., 2021), and both are expressed in U2OS cells. Therefore, we used Wnt3A as the FZD4 ligand. Wnt3A significantly increased ALP activity compared to the vehicle control (VC) (Fig. 1C). The endogenous chemokine ligand stromal derived factor-1α (SDF-1α) induced ERK1/2 phosphorylation through chemokine receptor, ACKR3 (Fig. 1D). Phospho-ERK1/2 levels were normalized to total ERK1/2 as shown on the immunoblot (Supplemental Fig. S2). Thus, we selected a dose of 10μM of CCPA, 200μM of PEA, 100ng/ml of Wnt3A and SDF-1α to selectively stimulate ADORA1, HRH1, FZD4, and ACKR3, respectively.

EV characterization from U2OS cells

First, we evaluated native U2OS EVs isolated from the culture media using ultrafiltration followed by size exclusion chromatography (SEC). The immunoblot revealed the presence of EV surface markers, tetraspanins CD9, CD63, and CD81 (Fig. 2A), in SEC fractions 7, 8, and 9. We also detected EV cytosolic markers syntenin (Kugeratski et al., 2021) and flotillin-1 in individual fractions 7-9. In addition, calnexin, an endoplasmic reticulum marker and a negative EV control, was absent in fractions 7-9 (Fig. 2A). All EV markers were absent in the media control sample, which suggested that the SEC fractions 7-9 were enriched in EVs from U2OS cells. The pooled EV-enriched fractions 7-9 were assessed for vesicle shape and size by TEM, which revealed vesicular structures ranging from 100-200 nm (Fig. 2B, red arrows). We quantified the EV concentration and size distributions using fluorescence nanoparticle tracking analysis (f-NTA), which enhances the detection of membrane vesicles by incorporation of a

fluorophore into the EV lipid membrane. The average concentration of EVs in U2OS culture supernatant was $6x10^9$ particles/mL (Fig. 2C, D), which was significantly increased compared to the media control. Despite using EV-depleted FBS, some residual bovine EVs, especially small-size EVs (Pham et al., 2021), remained in the media control, with an average concentration of $4.45x10^9$ particles/mL (Fig. 2C, D). However, they did not exhibit the EV markers we examined (Fig. 2A). Thus, those vesicles are most likely not derived from the host cell (Lehrich et al., 2021). Therefore, media control samples were included in all subsequent experiments to avoid any miRNA artifacts caused by serum. The size of EVs ranged from 50-500 nm with no significant difference in the median diameter between the media control (214 ±14.41nm) and U2OS-exposed media (237± 5.17 nm) (Fig. 2C). We also compared the EV concentration in various GPCR agonist treatment groups with their vehicle controls. Notably, the EVs from agonist-treated samples and vehicle controls exhibited similar concentration and size, with median diameter ranging from 210-240nm (Supplemental Fig. S3). Therefore, the pooled EV-enriched SEC fractions 7-9 were used for further miRNA assessment.

EV miRNAs differentially expressed following GPCR stimulation

We utilized high-throughput miRNA arrays to identify EV miRNA signatures following receptor activation. To analyze the EV miRNAs from stimulated receptors and avoid any confusion posed by the miRNA content in the media from non-stimulated cells, we excluded any miRNAs that were only present in the media control (Supplemental Table. S2) or were changed less than 10-fold (< 3.3 PCR cycles) between the media control and vehicle control. This allowed us to focus on analyzing specific receptor stimulation effects. We identified 105 miRNAs associated with ADORA1, 92 with HRH1, 88 with FZD4, and 86 with ACKR3 that expressed in at least 80% of either vehicle control or the agonist-treated samples and underwent statistical analysis. To further narrow down our miRNA of interest after receptor stimulation, we performed differential-expression testing using within-pairs linear regression and calculated *p*-values using a nonparametric rank-based (Skillings-Mack) test. This approach provided unbiased estimates of stimulation-treatment effects. We subsequently ranked the miRNAs within each

receptor type by magnitude of effect and selected all miRNAs with Skillings-Mack p-value < 0.2 for further investigation, emphasizing discovery power over avoidance of false positive results. Any miRNAs with absolute fold change ≥ 1.5 ($|\Delta\Delta Cq| \geq 0.585$) were chosen for enrichment analyses.

We directly compared the miRNAs expression across each receptor. The heat map illustrated distinct EV miRNA patterns unique to each receptor (Fig. 3A). Our analysis showed that 29 miRNAs were differentially expressed in the ADORA1 group compared to its vehicle control, with 10 miRNAs demonstrating an absolute fold change greater than 1.5 (Fig. 3B). Furthermore, 5 out of 10 miRNAs were observed with $p < 0.05$ (Table 1). For the HRH1 group, 3 out of 4 differentially expressed miRNAs were found to have $p < 0.05$ (Fig. 3C and Table 1). In contrast, among the 22 differentially expressed miRNA in FZD4 group, 10 exhibited an absolute fold change greater than 1.5 (Fig. 3D), but only one miRNA (miR-203a-3p) met the threshold of $p < 0.05$ (Table 1). A similar pattern was also observed in the ACKR3 group (Fig. 3E and Table 1). Additionally, we further assessed the shared and non-shared changes in miRNAs with at least 1.5-fold change in either direction for each receptor (Fig. 3F). We found that miR-550a-5p, miR-502-3p, miR-137, and miR-422a were the most changed miRNAs following ADORA1, HRH1, FZD4, and ACKR3 stimulation, respectively (refer to Supplemental Table S3 for a complete list of all differentially expressed miRNAs of individual receptors and raw data in data availability section).

MiRNA targets and pathway predictions following GPCR stimulation

We next performed target prediction and functional annotations on all miRNAs of interest that exhibited an absolute fold-change ≥ 1.5 (Fig. 3) for each receptor. For analysis involving multiple miRNAs, we selected gene targets predicted by at least two miRNAs for functional analysis through the Kyoto Encyclopedia of Genes and Genomes (KEGG) database. Following ADORA1 stimulation, we identified 3,562 miRNA predicted target genes, with 709 predicted genes targeted by at least two differentially regulated miRNAs. The top 25 enriched KEGG pathways associated with ADORA1 miRNA targets are

primarily related to cell proliferation, apoptosis, and cancer (Fig. 4A). After HRH1 stimulation, 357 predicted miRNA targets were selected for enrichment analysis. Many of the top predicted miRNA target enriched KEGG pathways were linked to various cancers (Fig. 4B). We observed significant enrichment of FoxO and ErbB signaling (Fig. 4B), which play crucial roles in angiogenesis, cell proliferation, apoptosis, and modulation of the immune response (Appert-Collin et al., 2015; Kim et al., 2022; Lam et al., 2013; Ryzhov et al., 2017), and are associated with HRH1 function (Fernández-Nogueira et al., 2018; Hatipoglu et al., 2023; Li et al., 2022). Additionally, we found that HRH1 miRNA predicted targets are enriched in endocrine and nervous system pathways. For instance, several hub genes identified in HRH1 miRNA target PPI network, such as PTEN, MYC, GSK3B, and SMAD3 (Supplemental Fig. S4), are known to be involved in insulin signaling (Cheung et al., 2010; Li et al., 2020; Patel et al., 2008; H. L. Wang et al., 2022). The most upregulated miRNA from HRH1 stimulation, miR-502-3p, was associated with multiple enriched pathways related to insulin resistance, including EGFR tyrosine kinase inhibitor resistance, AGE-RAGE signaling pathway in diabetic complications, and pancreatic cancer (Supplemental Fig. S5A). Overall, these findings suggest that altered miRNA expression following HRH1 activation may play a role in diabetes.

Generally, the miRNA targets of FZD4 were related to cancer, drug resistance, embryonic development, and aging (Fig. 4C). The most downregulated miRNA after FZD4 stimulation, miR-137, had targets that are enriched in GABAergic and dopaminergic synapses, suggesting its role in the regulation of synaptic function (Supplemental Fig. S5B). Additionally, miR-137 targets were linked to substance abuse and neurogenerative disease (Supplemental Fig. S5B). MiR-135b-3p and miR-422a exhibited increased expression following FZD4 and ACKR3 activation (Fig. 3D, 3E, and Supplemental Table S3). Therefore, some of the enriched pathways, including various cancer types and signaling pathways, shared similarities between two receptors (Fig. 4C and Fig. 4D). Alongside cancer-related pathways, several enriched pathways related to aging and neurodegenerative diseases, such as cellular senescence and autophagy were identified as ACKR3 miRNA targets (Fig. 4D). Insulin resistance-related pathways were also

observed when analyzing miRNA targets following ACKR3 stimulation (Fig. 4E). Note, however, that the top identified hub genes between the two receptors were distinct (Supplemental Fig. S4), suggesting FZD4 and ACKR3 may regulate the same cellular process through different mechanisms.

8. DISCUSSION

We hypothesized that stimulation of GPCRs can regulate the EV miRNA profile. We used a combined approach of ultrafiltration and SEC to isolate EVs from agonist-stimulated culture media, then followed up with miRNA qPCR arrays. Our findings provide evidence that within a single cell type, head-to-head comparisons of specific agonist-stimulation of GPCR subclasses reveal unique EV miRNA profiles.

Although various methods exist for isolating EVs, obtaining a high yield of pure EVs with minimal contamination is challenging (Sidhom et al., 2020). Combining ultrafiltration with SEC allowed us to isolate EVs with sufficient yield and purity, and that are suitable for further EV miRNA characterization. We noticed the median size of EVs measured by NTA was larger than the size reported by TEM. While f-NTA was utilized in this study to enhance membrane vesicle detection, it may not differentiate EVs from other similar particles, such as protein aggregates and lipoproteins. This overlap could lead to overestimating the EV size and impacting the accuracy of EV detection. Furthermore, this discrepancy could be due to EV storage and freeze-thaw cycles (Gelibter et al., 2022; Görgens et al., 2022). In contrast to freshly prepared samples for TEM, EV aggregation after the freeze-thaw cycle could result in increased particle size detected by NTA. Contrary to other studies that have reported increased EV release after GPCR stimulation (Ambrose et al., 2018; Conrad et al., 2020), we did not find significant changes in either the quantity or mean diameter between vehicle control and agonist-treated samples. We postulate that our EV production results could be due to the cell type and culture conditions (Bost et al., 2022; Palviainen et al., 2019). In addition, serum vesicles are a major source of EV contamination from the cell culture media. To minimize serum-derived EVs, our cells were cultured with EV-depleted FBS, which

may have a reduced ability to support cell growth (Bost et al., 2022). Therefore, different isolation methods and cell culture conditions could result in variations in EV concentrations.

Few studies have addressed GPCR activation and its stimulation of EV release in cultured cells (Alonso et al., 2011; Conrad et al., 2020; Mazzeo et al., 2016; F. J. Verweij et al., 2018), and indicating that GPCR signaling can regulate EV biogenesis and release. For instance, activation of (only) muscarinic receptor type I induces multivesicular body formation and stimulates EV secretion in T lymphocytes (Alonso et al., 2011). Similarly, stimulating (only) HRH1 promotes the exocytosis of multivesicular bodies in HeLa cells (Frederik Johannes Verweij et al., 2018). Conrad et al. demonstrated that activation of multiple endogenous GPCRs stimulates EV release from trophoblasts (Conrad et al., 2020). Moreover, numerous studies have shown that the activation of GPCRs regulates the expression of individual miRNAs. For example, activation of the estrogen receptor inhibits miR-148a levels in breast cancer cells and COX-2 induces miR-526b expression through the prostaglandin receptor, which promotes breast cancer progression (Majumder et al., 2015; Tao et al., 2015). However, the aforementioned studies did not investigate EV miRNA expression after GPCR stimulation. Ambrose et al. identified released miRNA patterns that are highly correlated with specific GPCR agonists in platelets (Ambrose et al., 2018). However, their miRNA analysis used EV-rich supernatant after GPCR stimulation, which included both non-EV and EV miRNAs. Here, we focused on EV miRNA profiles following GPCR stimulation. We found many of the EV miRNAs were similar across the four GPCR subgroups, although some unique miRNAs were associated with each receptor. We identified 10 miRNAs in ADORA1, 4 miRNAs in HRH1, 10 miRNAs in FZD4, and 6 miRNAs in ACKR3 that were differentially expressed following agonist stimulation. We found that a greater number of miRNAs showed increased expression levels compared to those with decreased expression after receptor activation. The increase in miRNAs ranged from 6 to 30% more than decreased miRNAs, depending on the specific receptor group. For example, following ADORA1 activation, there were about 15% more increased than decreased miRNAs, while in

the FZD4 group, there was a 6.3% higher number of increased miRNAs. Additionally, we observed a few miRNAs that exhibited more than a 1.5-fold change after each receptor activation. While endogenous miRNAs may be present in lower amounts in EVs, their functional significance can be considerable. Brown et al. demonstrated that a threshold concentration of miRNA is necessary to suppress target genes (Brown et al., 2007). This suggests that EV miRNAs may play a crucial role in miRNA expression in the recipient cells, helping them reach the required threshold to elicit specific effects.

Our study directly compared the stimulation of specific GPCR subclasses and the unique EV miRNA signatures that might dictate downstream $G\alpha_i$, $G\alpha_q$, $G\alpha_{12/13}$, and β-arrestin protein cascades. G proteins transduce the extracellular signals to the appropriate downstream effectors. Multiple GPCRs can couple to the same type of G protein. One GPCR also can interact with different G proteins to trigger multiple pathways. Previous reports showed that overexpression of Gα12 can alter multiple miRNA levels (Yang et al., 2015), suggesting that G proteins may play a role in controlling miRNA expression after GPCR stimulation. Despite our result suggesting a unique miRNA signature for each receptor, it is not clear that a miRNA signature was associated with specific types of G proteins due to the limited sample size (four receptors). Future studies are necessary to resolve whether EV miRNAs are regulated by specific G proteins after GPCR stimulation.

When we compared the predicted functional effects of EV miRNAs across the four GPCRs, we found that numerous enriched pathways were associated with human cancers. For instance, the targets of HRH1 miRNA were enriched in colorectal cancer, breast cancer, and melanoma, which were consistent with previous findings (Li et al., 2022; Park et al., 2023; Shi et al., 2019). This could be because many of the predicted miRNA targets that are involved in a wide range of cellular activities, such as cell proliferation, differentiation, migration, and apoptosis, that contribute to cancer initiation, progression and metastasis

(Evan & Vousden, 2001; Matthews et al., 2022; Pfeffer & Singh, 2018). Additionally, the top hub genes identified in the PPI network of FZD4 miRNA targets, including MYC, EGFR, MDM2, and CDK1 (Supplemental Fig. S4), were also involved in many aspects of cancer progression (Gabay et al., 2014; Oliner et al., 2016; Sigismund et al., 2018; Wang et al., 2023). This finding may contribute to understanding the mechanism of GPCR activities in cancer progression and to the development of new pharmacotherapies.

Moreover, our data revealed functional differences among the four GPCRs. When we compared the differentially expressed miRNAs and their predicted pathways across four GPCRs, we found ADORA1 had a unique set of miRNAs that did not overlap with the other 3 GPCRs. Three significantly altered ADORA1 miRNAs, miR-135a-5p, miR-31-5p, and miR-454-3p, are associated with cardioprotection (Chen et al., 2022; Liu et al., 2024; Wang et al., 2021; Zhao et al., 2024), supporting the established role of ADORA1 in the protection of cardiomyocytes during ischemia (Crawford et al., 2005; Reichelt et al., 2005). We observed that several insulin-resistant pathways were enriched among the targets of HRH1 miRNAs. The two significantly elevated HRH1 miRNAs, miR-502-3p and miR-423-5p, affect glucose metabolism (Liu et al., 2023; Montastier et al., 2019; Yang et al., 2017). Notably, miR-423-5p has been identified as a potential biomarker of severe obesity (Ortega et al., 2013). Consistent with previous studies (Shi et al., 2019; Wang et al., 2010), our findings indicate that HRH1 may play a role in regulating insulin sensitivity. MiR-137 and miR-518e-3p were solely expressed in EVs from cells treated with FZD4 agonist, and not after activation of other receptors, suggesting they may serve as unique signatures of FZD4 activation. Interestingly, genome-wide association and proteomic studies have implicated the *MIR137* host gene, and the mRNA targets of miR-137 are risk genes for schizophrenia (Palumbo et al., 2023; Ripke et al., 2014). Although the FZDs activation mechanism and FZDs-G protein interaction are still not fully understood (Arthofer et al., 2016; Strakova et al., 2017; Zhang et al., 2024), this study could lead to the identification of new miRNA targets for GPCR activation and post-transcriptional mRNA

gene targets as a down-stream effector for rational drug design. The predicted pathways for ACKR3 miRNA indicated that 9 of the top 25 significantly enriched pathways were associated with aging and neurodegenerative diseases. Cell senescence, which is a permanent cell growth arrest and linked to aging and several neurodegenerative disorders (Kritsilis et al., 2018; Papadopoulos et al., 2020; Suelves et al., 2023), was observed with the highest gene count among those pathways. Additionally, miR-135b, the only significantly increased ACKR3 miRNA, promotes hippocampal cell proliferation and enhances learning and memory by affecting the rate-limiting enzyme for β-amyloid production. miR-135b is significantly reduced in the peripheral blood of Alzheimer's disease patients (Zhang et al., 2016). GPCRs play a significant role in various diseases through different mechanisms of action. Our study suggests that the alteration of specific miRNA expression following GPCR activation by pharmacotherapies may introduce a new mechanism through which GPCRs regulate extracellular events by modulating the expression of miRNAs in EVs.

This study highlights the novel mechanism of EV miRNA content regulated by GPCRs. However, there are limitations in the current study. The EVs used for miRNA analysis are a heterogeneous population, of various but similar sizes, and may originate from different biogenesis pathways and exhibit distinct biological functions. GPCR agonists (or vehicle) may stimulate production of different subclasses of the EVs, such as exomeres, exosomes, or even microvesicles, and affect their content. Further experiments with optimized isolation methods are needed to investigate changes in EV subpopulations and miRNAs regulated by GPCRs. U2OS cells expressing endogenous GPCRs were used as a model to explore EV miRNA profiles. Thus, the differentially expressed miRNAs detected in the current study could be cell-type specific. EV content and miRNA expression could vary by cell type and culture conditions. EV miRNA expression after receptor stimulation in different cell lines should be further explored. In this exploratory study, we used bioinformatics to predict the target genes and enriched pathways of the differentially expressed miRNAs following GPCR activation. Future directions should experimentally

validate the differentially expressed miRNAs and their gene targets, as well as assess the functional consequences.

In summary, we characterized EV miRNA profiles from U2OS cells after stimulation of specific GPCR subclasses with selective agonists. We identified unique EV miRNA signatures resulting from GPCR subtype activation. The functional analyses revealed that the predicted gene targets of the EV miRNAs were enriched in distinct metabolic pathways, including physiological and pathological states of cell function. This study offers a novel biological mechanism, EV miRNA content regulation by stimulated GPCRs, and provides insight for future studies of drug-receptor interactions including unwanted and unintended effects.

9. MATERIALS AND METHODS

Key Resources Table				
Reagent type (species) or resource	**Designation**	**Source or reference**	**Identifiers**	**Additional information**
Cell line (*Homo-sapiens*)	U2 OS (epithelial, osteosarcoma)	ATCC	HTB-96	
Antibody	Rabbit polyclonal anti-Flotillin1	Abcam	Ab41927	1:1000
Antibody	Rabbit monoclonal anti- Syntenin	Abcam	Ab133267	1:1000
Antibody	mouse monoclonal anti-CD63	Santa Cruz Biotechnology	sc-5275	1:1000

Antibody	mouse monoclonal anti-CD81	Santa Cruz Biotechnology	sc-166029	1:500
Antibody	Rabbit polyclonal anti-CD9	Abcam	ab223052	1:1000
Antibody	Rabbit polyclonal anti-calnexin	Abcam	ab22595	1:1000
Antibody	Rabbit monoclonal anti-phospho-ERK1/2 (pERK1/2)	MilliporeSigma	05-797R	1:1000
Antibody	Rabbit polyclonal anti-p44/42 MAPK (total ERK1/2)	Cell Signaling Technology	9102	1:1000
Antibody	Mouse monoclonal anti-β-actin	Santa Cruz Biotechnology	sc-69879	1:1000
sequence-based reagent	Megaplex RT primer human pool set V3.0	Thermo Fisher Scientific	4444750	
sequence-based reagent	Megaplex PreAmp primers human pool set V3.0	Thermo Fisher Scientific	4444748	
sequence-based reagent	TaqMan Array Human MicroRNA A+B Card Set v3.0	Thermo Fisher Scientific	4444913	
peptide, recombinant protein	Human recombinant SDF-1α	MilliporeSigma	GF344	
peptide, recombinant protein	Human recombinant Wnt3a	MilliporeSigma	H17001	

Commercial assay or kit	cAMP EIA kit	Cayman Chemical	581001	
Commercial assay or kit	ALP assay kit	Abcam	ab83369	
Commercial assay or kit	Cisbio IP-1 Elisa kit	Revvity	72IP1PEA	
Commercial assay or kit	MagMax mirVana total RNA isolation kit	Applied Biosystems, Thermo Fisher Scientific	A27828	
Commercial assay or kit	Qubit miRNA assay kit	Thermo Fisher Scientific	Q32880	
Chemical compound, drug	Di8-ANEPPS	Thermo Fisher Scientific	D3167	
Chemical compound, drug	Fluronic F-127	Thermo Fisher Scientific	P3000MP	
Chemical compound, drug	2-Chloro-N^6-cyclopentyladenosine (CCPA)	Tocris Bioscience	1705	
Chemical compound, drug	8-Cyclopentyl-1,3-dipropylxanthine (DPCPX)	Tocris Bioscience	0439	
Chemical compound, drug	2-pyridylethylamine dihydrochloride	Tocris Bioscience	2478	
Chemical compound, drug	Cetirizine dihydrochloride	Tocris Bioscience	2577	

software, algorithm	GraphPAD Prism software version 10	GraphPAD Software Inc.		
software, algorithm	SR plot web service	https://www.bioinformatics.com.cn/srplot		
software, algorithm	miRNet online web service v2.0	http://www.mirnet.ca		
software, algorithm	CytoScape software (V3.10.1)	https://cytoscape.org		

Drugs and reagents

CCPA, the selective adenosine A_1 receptor agonist, and adenosine A_1 receptor antagonist, DPCPX, were obtained from Tocris Bioscience (Minneapolis, MN). 2-pyridylethylamine dihydrochloride (PEA), the agonist of the histamine H_1 receptor, and cetirizine dihydrochloride, the antagonist of H_1 receptor were obtained from Tocris Bioscience (Minneapolis, MN). CCPA and DPCPX were diluted in DMSO, then subsequently diluted in the cell culture medium with a final DMSO concentration of 0.01%. Both 2-pyridylethylamine dihydrochloride and cetirizine dihydrochloride were diluted in water. Human recombinant Wnt3a protein and SDF-1α were obtained from Sigma (Burlington, MA). Wnt3a and SDF-1α were reconstituted to 100μg/ml in sterile 1XPBS containing 0.1% human serum albumin (HSA) at 100μg/ml. Wnt3a and SDF-1α were subsequently diluted in the cell culture medium with a final HSA concentration of 0.0001%. Gibco exosome-depleted fetal bovine serum (FBS) was purchased from ThermoFisher (A2720801, Thermo Fisher Scientific, Waltham, MA). Then the FBS were further charcoal-stripped to remove the potential GPCR agonists in the serum.

Cell culture

U2OS cells purchased from ATCC (Cat. No. HTB-96) were grown in McCoy 5A medium (16600082, Gibco, Thermo Fisher Scientific) supplemented with 10% fetal clone serum (FCS) and 1% penicillin and streptomycin and maintained in a humidified incubator with 10% CO_2 according to ATCC instructions. For EV isolation, cells were plated at $6x10^6$ in a 15 cm culture dish two days before the experiment. On the day of the experiment, cells were rinsed with 1XPBS, then treated with agonists or vehicle control in the medium containing 10% EV-depleted and charcoal-stripped FBS. The treatments were left on for 24 hours before medium collection for EV isolation. Four 15 cm plates with a total medium volume of 55 ml of each condition were used for EV isolation.

cAMP accumulation assay

U2OS cells were plated at $4x10^5$/well in the 24-well plate two days before the assay. One day before the assay, cells were switched to the culture medium containing 10% charcoal-stripped FCS and incubated overnight. The assay procedure and buffer are as previously described (Watts et al., 1998). CCPA (10^{-9} to 10^{-4}) was added to the cells and the plates were incubated for 20 min at 37°C in a humidified incubator with 5% CO_2. For the experiment with the antagonist, DPCPX (5 μM) was added to the cells and preincubated for 10 min before CCPA addition. cAMP accumulation was measured using cAMP EIA kit from Cayman Chemical (581001, Ann Arbor, MI), according to the manufacturer's instructions. All the experiments were conducted with three biological repeats, each performed with duplicated determinants.

Inositol monophosphate formation

U2OS cells were plated at $4x10^5$/well in the 24-well plate one day before the assay in the culture medium containing 10% charcoal-stripped FCS. The next day, cells were starved with plain McCoy 5A medium for 1 hour before the assay. Cells were preincubated with stimulation buffer for 10 min before agonist addition. Pyridylethylamine (10^{-8} to 10^{-3}) was added to the cells and the plates were incubated for 60min at 37°C in a humidified incubator with 5% CO_2. For the experiment with the antagonist, Cetirizine (1 μM) was preincubated for 10min before agonist addition. The accumulation of inositol monophosphate was

measured using the Cisbio IP-1 Elisa kit (72IP1PEA, Revvity, Waltham, MA) as described previously (Eshleman et al., 2013). All the experiments were conducted with three independent repeats, each performed with duplicate determinants.

Alkaline phosphatase assay

U2OS cells were seeded at $4x10^5$/well in the 12 well-plate one day before the agonist treatment. Cells were treated with vehicle control (HSA) or various doses of Wnt3a diluted in cell culture medium and incubated for 24 hours. On the day of the assay, cells were rinsed with ice-cold 1XPBS and kept on the wet ice all the time. Cells were scraped and collected with 100 µl assay buffer/well, then transferred to microcentrifuge tubes. The cell suspensions were homogenized for 15-20 seconds with the micro pestle homogenizer. The lysates were centrifuged 13,000xg for 20 min at 4°C to remove insoluble material. Alkaline phosphatase (ALP) activity was measured using the ALP assay kit (ab83369, Abcam, Waltham, MA). Briefly, 80 µl of cell lysate aliquot/well was mixed with kit reagent, then the plate was incubated at 25°C for 60 min. 10 µl of cell lysate was used to measure total protein concentration, which is used to normalize the enzyme activity. All the experiments were conducted with three independent repeats, each performed with duplicate determinants.

EV isolation by size exclusion chromatography

To determine which fractions are EV-enriched, 30ml of the medium control (plain medium with 10% EV-depleted FBS) and 30ml of the conditioned medium from two 15cm plates of U2OS cells incubated for 24 hours were collected and centrifuged at 300xg at 4°C for 15 min to remove cells and cell debris. The EV isolation methods were adapted from Benedikter et al 2017 (Benedikter et al., 2017). The supernatants were collected and centrifuged at 4000xg at 4°C for 15 min to further remove cell debris. After the second spin, the supernatants were passed through a 0.22µM Millipore Steriflip filter (Burlington, MA). Then media were loaded on a 2% Tween precoated Amicon Ultra-15 centrifugal filter unit with Ultracel-10 membrane (MWCO=10kDa, Millipore, Burlington, MA). The media were concentrated to ~550 µl by

repeated centrifuge (4000xg) at 4°C. The concentrated media were fractionated by using size exclusion chromatography (SEC) (Izon qEV Original/35nM, IZON Science, Medford, MA) according to the manufacturer's instructions. Briefly, 500 µl of concentrated media were loaded to the qEV column. 12 fractions of 0.5 ml each eluted with 1XPBS (0.1uM filtered) were collected. Individual fractions were concentrated with Microcon-30 kDa Centrifugal Filters (Millipore, Burlington, MA) to a final volume of 70 µl and stored at -80°C for immunoblot.

For further miRNA assessment, 60ml of conditioned media pooled from four 15 cm plates per condition were harvested after 24 hours incubation of U2OS cells with agonists or vehicle control. For each GPCR, the experiments included 6 replicates of the agonist treatment group, 6 replicates of vehicle control (VC) and 6-8 replicates of media control (MC). The EV-enriched fractions 7, 8, and 9 (with a total volume of 1.5ml) were pooled for transmission electron microscopy (TEM), nanoparticle tracking analysis (NTA) and total RNA isolation. Pooled fractions were aliquoted and stored at -80°C until processed. Fractions used for TEM were stored at 4°C.

Immunoblotting

To evaluate the EV-enriched SEC fractions, 500µl of void (pooled fraction 1-6) and individual fractions 7 to 12 were concentrated with Microcon-30 kDa Centrifugal Filters (Millipore, Burlington, MA) to a final volume of 70 µl. Due to the undetectable protein amount in the concentrated fractions, an equal volume (30 µl) for each fraction was subjected to SDS-PAGE through 12% polyacrylamide gels and transferred to polyvinylidene fluoride (PVDF) membranes (BioRad, Hercules CA). Membranes were blocked with 5% non-fat dry milk in TBST at room temperature for 30 min, and then subsequently incubated at 4°C overnight with rabbit anti-flotillin (1:1000, ab41927, Abcam, Waltham, MA), rabbit anti-syntenin (1:1000, ab133267, Abcam, Waltham, MA), mouse anti-CD63 (1: 1000, sc-5275, Santa Cruz Biotechnology), mouse anti-CD81(1:500, sc-166029, Santa Cruz Biotechnology), rabbit anti-CD9 (1: 1000, ab223052, Abcam, Waltham, MA), rabbit anti-calnexin (1:1000, ab22595, Abcam, Waltham, MA). The immunoblots were rinsed and incubated with HRP-conjugated secondary antibodies. Immune

complexes were visualized by chemiluminescence and analyzed using Bio-Rad ChemiDoc Imager. Bands were analyzed by densitometry using Bio-Rad Image lab software.

For the ACKR3 functional assay, cell lysates with a total of 15 µg protein of each condition were loaded into the gel. The immunoblots were incubated overnight with rabbit anti-pERK1/2 (1:1000, 05-797R, MilliporeSigma, Burlington MA), rabbit anti-tERK1/2 (1:1000, 9102, Cell Signaling Technology, Danvers MA), and mouse anti-β-actin (1:1000, sc-69879, Santa Cruz Biotechnology, Dallas Texas). β-actin was used as an internal control.

Transmission electron microscopy of EVs

15 µl of EV pooled fractions 7 to 9 were mixed with 5 µl of 16% paraformaldehyde and kept on the wet ice until processed. 5 µl of EV preparations were deposited and incubated for 3 minutes onto glow discharged copper grids (Ted Pella 01822-F). After this incubation period the grids were rinsed 15 seconds in distilled water, wicked on Whatman filter paper #1, and then stained for 3 minutes in freshly prepared 1% (w/v) aqueous uranyl acetate. Grids were then wicked with filter paper and air dried. Samples containing EVs were imaged at 120 kV on a FEI Tecnai™ Spirit TEM system. Images were acquired on an Advanced Microscopy Techniques (AMT) Nanosprint12 cMOS 12-megapixel camera system as tiff files.

Fluorescence nanoparticle tracking analysis (f-NTA)

SEC EVs (pooled void volume fraction1-6 and pooled EV enriched fraction 7-9) from controlled media and media from U2OS cells were analyzed for particle concentration and size by ZetaView nanoparticle tracking analyzer (Particle Metrix, Ammersee Germany) as described by the manufacture's protocol. Briefly, EV samples were labeled with fluorescent membrane dye Di8-ANEPPS (D3167, Thermo Fisher Scientific, Waltham, MA), staining solution (12 µM) supplemented with Fluronic F-127 (P3000MP Thermo Fisher Scientific, Waltham, MA) at room temperature for 15 min. The samples were diluted at 1:200 in 0.1 µM filtered 0.1X PBS in a final volume of 1ml for injection. Before the measurement, the instrument was calibrated with 100 nm polystyrene beads (Particle Metrix, Cat no 110-0020). The EV

samples were recorded for 90s at controlled room temperature. All measurements were done in triplicates. ZetaView software was used to quantify the concentration (particles/ml) and size distribution (nm) of the particles.

EV RNA isolation and miRNA array

Pooled EV-enriched fractions (7,8 and 9, total of 1.3ml) were concentrated with Microcon-30 kDa Centrifugal Filters (Millipore, Burlington, MA) to a final volume of 250 µl and used for EV RNA isolation. The total RNAs were isolated using MagMax mirVana total RNA isolation kit (A27828, Applied Biosystems, ThermoFisher Scientific) according to manufacturer's instructions. The miRNA concentration of each sample was measured with the Qubit miRNA assay kit (Q32880, ThermoFisher Scientific). The isolated RNA was stored at -80°C until processing. The reverse transcription and pre-amplification reactions were run as previously described (Sandau et al., 2020). Briefly, RNA (with 8-10 ng of miRNA) was reverse transcribed using Megaplex RT primer human pool set V3.0 (4444750, ThermoFisher Scientific) and MultiScribe Reverse Transcriptase (4311235, ThermoFisher Scientific) according to the user guide. To increase the sensitivity of qPCR analysis for miRNA targets, cDNA was pre-amplified (14 cycles) with Megaplex PreAmp primers human pool set V3.0 (4444748, ThermoFisher Scientific) and TaqMan PreAmp Master mix (4391128, ThermoFisher Scientific). Before the qPCR, pre-amplified cDNA was diluted 1:1 in nuclease-free water, then mixed with TaqMan Universal Master Mix (444047, ThermoFisher Scientific). The samples were loaded to TaqMan Array Human MicroRNA A+B Card Set v3.0 (4444913, ThermoFisher Scientific), which contains a total of 754 miRNA assays. The PCR amplification and data acquisition were carried out using the QuantStudio 12K Flex real-time PCR system (ThermoFisher Scientific).

miRNA array and analysis

MiRNA expression was analyzed using relative quantification methods as previously described (Sandau et al., 2020). The Cq value for each well along with the amplification score (AmpScore) and Cq

confidence (CqConf) was reported by ExpressionSuit Software v1.3 (ThermoFisher). Amplifications were filtered prior to the data analysis, as follows: PCR products with Cq > 34, CqConf < 0.8, or AmpScore < 1 were excluded and treated as missing values. Only expressed miRNAs meeting these criteria in more than 80% of both vehicle control and treatment group samples were accepted for further analysis. To maximize accuracy and minimize amplification variation between the A and B cards, a mean expression value calculated from qualified miRNAs pooled from both the A and B cards was used to normalize the PCR data. miRNAs chosen for calculating mean expression for endogenous background normalization had to meet the following criteria: (1) the miRNA was not expressed or was observed in less than 50% of the untreated media, (2) was consistently fully observed in all vehicle control and treated samples and (3) for miRNAs observed at rates of less than 50% in untreated media, the Cq value of the media control was required to be > 3.3 cycles different from the vehicle control. The mean expression Cq value of all the qualified miRNAs was calculated and used for endogenous background normalization. The ΔCq value for a miRNA was calculated as: ΔCq = Cq value of the miRNA – mean normalizer Cq value in the same group. The ΔΔCq value for a miRNA was calculated as: ΔΔCq = ΔCq for treated samples – ΔCq for vehicle control samples. The fold change (relative quantification value) for each miRNA was calculated as: $2^{-\Delta\Delta Cq}$. A relative quantification value > 1 indicates increased miRNA expression in the treated samples compared to vehicle control, and a relative quantification value < 1 indicates decreased miRNA expression in the treated samples.

Data analysis and statistical analysis

Dose-response curves for cAMP and IP1 accumulation were analyzed by nonlinear regression. Significant differences were determined by two-way analysis of variance (ANOVA) of receptors by agonist or antagonist concentration followed by Sidak's multiple comparison test. For the ALP accumulation and ERK1/2 activation, the significant differences were assessed by one-way ANOVA followed by Tukey's multiple comparison test. All functional assay data were shown as mean ± SD. The statistical significance in EV concentrations was determined using Student's *t*-test. Data were expressed as mean ±

SEM. Data were analyzed with GraphPAD Prism software v10 (GraphPAD Software Inc., San Diego, CA). Statistical tests were applied based on three independent replicates. P values < 0.05 were considered significant.

To statistically evaluate the qPCR miRNA expression data, we elected to use strongly unbiased robust procedures including matched-pairs estimators of the effect sizes and rank-based testing of associations in the interest of minimizing confounding of associations by technical causes, and then to further interrogate those results with extensive sensitivity analyses designed to probe the volatility of the conclusions depending on our choice of analytical methods. For example, as an alternative normalization procedure to relax the assumption (needed for validity of per-run normalization) of no differential measurement drift and to mitigate the run-to-run volatility of normalizer mean estimation we considered aligning median normalizer scores by treatment group rather than explicitly adjusting qPCR runs for each sample, but observed that residual technical variance (in the aligned normalizer scores) between matched pairs was actually increased due to the complications of missing data created by quality filtering, the technical run-batching of the assay into A and B cards, varying qPCR performance of even the endogenous normalizer miRNAs across runs, and other technical factors beyond our control.

To estimate the treatment effects on miRNA and calculate robust p-values for testing of those effects, we considered six different combinations of treatment effect estimator and p-value estimator in sensitivity analyses (Supplemental Fig. S1); Each of the approaches offers an alternative estimate of the magnitude and significance of the ΔΔCq value, varying depending on how pairs and treatment groups and batches are aggregated or disaggregated. We consider the matched-pairs estimator (Allison, 2009) of treatment effect superior to other approaches because of its strong unbiasedness even in the presence of technical confounding, and the Skillings-Mack estimator (Skillings & Mack, 1981) of the p-value superior both to

naïve permutation-based (Good, 2006) or rank-based tests (Mann & Whitney, 1947) and to Welch's robust t-test (Welch, 1947) because it explicitly accounts for imbalanced group sizes (in our case caused by missing data at the per-miRNA level).

Ranking of miRNAs within each receptor type was first performed by magnitude of treatment effect (in normalized ΔCq units), as estimated from the matched-pairs regression approach, and the ranking was then filtered by the Skillings-Mack p-value. Because of the first-in-practice exploratory nature of this study we opted to emphasize discovery power over avoidance of false positives, and thus chose a liberal cutoff of $p < 0.2$ for selection of associated miRNAs for further investigation. Pathway enrichment and functional annotation analyses were limited to the subset of miRNAs highlighted as the most-affected for each receptor; the cutoff for this was absolute fold change ≥ 1.5 ($|\Delta\Delta Cq| \geq 0.585$) for agonist versus vehicle control. The $\log_2$ fold change, Skillings-Mack p-values, and z-transformed $\log_2$ fold change values (Z-Score) were used to create volcano plots and hierarchical heatmaps. The hierarchical clustering in the heatmap is based on Euclidean distance. The visualizations were generated using GraphPad Prism v.10 and SR plot web service (https://www.bioinformatics.com.cn/srplot).

miRNA targets and pathway analysis

Prediction of miRNA targets was conducted using miRNet online web service v2.0 (http://www.mirnet.ca). The miRNA-target interactions were analyzed using the experimentally validated miRNA-target interaction databases: miRTarbase (v8.0) and Tarbase (v8.0). Human transcripts targeted by at least two miRNAs from each receptor were exported for further functional analysis. The target gene lists were submitted to String (v12.0) and GeneOntology with default settings to identify pathways enriched with miRNA targets and construct PPI networks. Kyoto Encyclopedia of Genes and Genomes (KEGG) pathway enrichment analyses and WikiPathway analyses were performed with String (v12.0)

using the hypergeometric algorithm and the statistically enriched terms were determined by Fisher's exact test with adjusted *p*-value (false discovery rate) < 0.05 as the threshold. To measure the enrichment effect, the pathways were sorted by $\log_{10}$(observed/expected), which is the ratio between the number of proteins in our observed network that are annotated with a term and the number of the proteins that the software expects to be annotated with the same term in a random network of the similar size. Pathways exhibiting significant changes were further visualized with bubble plots using the SR plot web service (https://www.bioinformatics.com.cn/srplot). The PPI networks constructed by String were analyzed with CytoScape software (V3.10.1). The hub genes were identified and selected using CytoHubba, a plug-in of CytoScape, according to the node degree in the PPI network.

10. ACKNOWLEDGEMENTS: We thank Dr. Alfred Lewy, Dr. Kim Neve, and Dr. Atheir Abbas for critically reading the manuscript. We also acknowledge the OHSU Gene Profiling Shared Resource for providing the technical support for the qPCR assays. Transmission electron microscopy was performed at the Multiscale Microscopy Core, a member of the OHSU University Shared Resource Cores (RRID:SCR_022652) under the guidance of Dr. Claudia S. Lopez.

11. DATA AND MATERIALS AVAILABILITY: The microRNA array data is MIAME compliant and have been deposited to the Gene expression Omnibus site: http:// www.ncbi.nlm.nih.gov/geo/. GEO accession numbers: GSE270077, GSE270078, GSE270079, and GSE270080. All data needed to evaluate the conclusions in the paper are present in the paper or in the Supplemental Materials. Materials are available upon request from the corresponding author.

12. AUTHOR CONTRIBUTIONS: Conceptualization, X.S., M.C.P, and A.J.; investigation and methodology X.S., M.C.P, S.B., J.W., S.M., and A.J.; manuscript writing, editing, and reviewing X.S., M.C.P, S.B., J.W., S.M., and A.J.; funding acquisition A.J.

13. FOOTNOTE

Funding: This work was supported by funding from T32AG055378-06 (M.C.P), NIDA ADA 12013 (A.J.), FDA CDER-20-I—0546 (A.J.), DEA D-15-0D-002 (A.J.), Department of Veterans Affairs 1IK6BX005754 (A.J.). Illustrations were created with BioRender.com.

Competing Interests: The authors declare that they have no competing interests.

14. REFERENCES

Allison, P. (2009). *Fixed Effects Regression Models* https://doi.org/10.4135/9781412993869

Alonso, R., Mazzeo, C., Rodriguez, M. C., Marsh, M., Fraile-Ramos, A., Calvo, V., Avila-Flores, A., Merida, I., & Izquierdo, M. (2011). Diacylglycerol kinase α regulates the formation and polarisation of mature multivesicular bodies involved in the secretion of Fas ligand-containing exosomes in T lymphocytes. *Cell Death & Differentiation*, *18*(7), 1161-1173. https://doi.org/10.1038/cdd.2010.184

Ambrose, A. R., Alsahli, M. A., Kurmani, S. A., & Goodall, A. H. (2018). Comparison of the release of microRNAs and extracellular vesicles from platelets in response to different agonists. *Platelets*, *29*(5), 446-454. https://doi.org/10.1080/09537104.2017.1332366

Appert-Collin, A., Hubert, P., Crémel, G., & Bennasroune, A. (2015). Role of ErbB Receptors in Cancer Cell Migration and Invasion. *Front Pharmacol*, *6*, 283. https://doi.org/10.3389/fphar.2015.00283

Arthofer, E., Hot, B., Petersen, J., Strakova, K., Jäger, S., Grundmann, M., Kostenis, E., Gutkind, J. S., & Schulte, G. (2016). WNT Stimulation Dissociates a Frizzled 4 Inactive-State Complex with Gα12/13. *Mol Pharmacol*, *90*(4), 447-459. https://doi.org/10.1124/mol.116.104919

Asher, W. B., Terry, D. S., Gregorio, G. G. A., Kahsai, A. W., Borgia, A., Xie, B., Modak, A., Zhu, Y., Jang, W., Govindaraju, A., Huang, L. Y., Inoue, A., Lambert, N. A., Gurevich, V. V., Shi, L., Lefkowitz, R. J., Blanchard, S. C., & Javitch, J. A. (2022). GPCR-mediated β-arrestin activation deconvoluted with single-molecule precision. *Cell*, *185*(10), 1661-1675.e1616. https://doi.org/10.1016/j.cell.2022.03.042

682 Bebelman, M. P., Crudden, C., Pegtel, D. M., & Smit, M. J. (2020). The Convergence of Extracellular
683 Vesicle and GPCR Biology. *Trends Pharmacol Sci*, *41*(9), 627-640.
684 https://doi.org/10.1016/j.tips.2020.07.001
685 Benedikter, B. J., Bouwman, F. G., Vajen, T., Heinzmann, A. C. A., Grauls, G., Mariman, E. C., Wouters, E.
686 F. M., Savelkoul, P. H., Lopez-Iglesias, C., Koenen, R. R., Rohde, G. G. U., & Stassen, F. R. M.
687 (2017). Ultrafiltration combined with size exclusion chromatography efficiently isolates
688 extracellular vesicles from cell culture media for compositional and functional studies. *Sci Rep*,
689 *7*(1), 15297. https://doi.org/10.1038/s41598-017-15717-7
690 Bhattacharya, P., Dhawan, U. K., Hussain, M. T., Singh, P., Bhagat, K. K., Singhal, A., Austin-Williams, S.,
691 Sengupta, S., & Subramanian, M. (2023). Efferocytes release extracellular vesicles to resolve
692 inflammation and tissue injury via prosaposin-GPR37 signaling. *Cell Rep*, *42*(7), 112808.
693 https://doi.org/10.1016/j.celrep.2023.112808
694 Bost, J. P., Saher, O., Hagey, D., Mamand, D. R., Liang, X., Zheng, W., Corso, G., Gustafsson, O., Görgens,
695 A., Smith, C. E., Zain, R., El Andaloussi, S., & Gupta, D. (2022). Growth Media Conditions
696 Influence the Secretion Route and Release Levels of Engineered Extracellular Vesicles. *Adv*
697 *Healthc Mater*, *11*(5), e2101658. https://doi.org/10.1002/adhm.202101658
698 Bourgeois, B. L., Levitt, D. E., Molina, P. E., & Simon, L. (2023). Differential expression of adipocyte and
699 myotube extracellular vesicle miRNA cargo in chronic binge alcohol-administered SIV-infected
700 male macaques. *Alcohol*, *108*, 1-9. https://doi.org/10.1016/j.alcohol.2022.11.001
701 Brown, B. D., Gentner, B., Cantore, A., Colleoni, S., Amendola, M., Zingale, A., Baccarini, A., Lazzari, G.,
702 Galli, C., & Naldini, L. (2007). Endogenous microRNA can be broadly exploited to regulate
703 transgene expression according to tissue, lineage and differentiation state. *Nature*
704 *Biotechnology*, *25*(12), 1457-1467. https://doi.org/10.1038/nbt1372
705 Chao, Y., Gu, T., Zhang, Z., Wu, T., Wang, J., & Bi, Y. (2023). The role of miRNAs carried by extracellular
706 vesicles in type 2 diabetes and its complications. *J Diabetes*. https://doi.org/10.1111/1753-
707 0407.13456
708 Chen, H., Qiao, H., Zhao, Q., & Wei, F. (2022). microRNA-135a-5p regulates NOD-like receptor family
709 pyrin domain containing 3 inflammasome-mediated hypertensive cardiac inflammation and
710 fibrosis via thioredoxin-interacting protein. *Bioengineered*, *13*(3), 4658-4673.
711 https://doi.org/10.1080/21655979.2021.2024956
712 Cheung, L., Zervou, S., Mattsson, G., Abouna, S., Zhou, L., Ifandi, V., Pelengaris, S., & Khan, M. (2010). c-
713 Myc directly induces both impaired insulin secretion and loss of β-cell mass, independently of
714 hyperglycemia in vivo. *Islets*, *2*(1), 37-45. https://doi.org/10.4161/isl.2.1.10196
715 Conrad, K. P., Tuna, K. M., Mestre, C. T., Banwatt, E. S., & Alli, A. A. (2020). Activation of multiple
716 receptors stimulates extracellular vesicle release from trophoblast cells. *Physiol Rep*, *8*(20),
717 e14592. https://doi.org/10.14814/phy2.14592
718 Crawford, M., Ford, S., Henry, M., Matherne, G. P., & Lankford, A. (2005). Myocardial function following
719 cold ischemic storage is improved by cardiac-specific overexpression of A1-adenosine receptors.
720 *Can J Physiol Pharmacol*, *83*(6), 493-498. https://doi.org/10.1139/y05-038
721 Doyle, L. M., & Wang, M. Z. (2019). Overview of Extracellular Vesicles, Their Origin, Composition,
722 Purpose, and Methods for Exosome Isolation and Analysis. *Cells*, *8*(7).
723 https://doi.org/10.3390/cells8070727
724 Eshleman, A. J., Wolfrum, K. M., Hatfield, M. G., Johnson, R. A., Murphy, K. V., & Janowsky, A. (2013).
725 Substituted methcathinones differ in transporter and receptor interactions. *Biochem Pharmacol*,
726 *85*(12), 1803-1815. https://doi.org/10.1016/j.bcp.2013.04.004
727 Evan, G. I., & Vousden, K. H. (2001). Proliferation, cell cycle and apoptosis in cancer. *Nature*, *411*(6835),
728 342-348. https://doi.org/10.1038/35077213

729 Fernández-Nogueira, P., Noguera-Castells, A., Fuster, G., Recalde-Percaz, L., Moragas, N., López-Plana,
730 A., Enreig, E., Jauregui, P., Carbó, N., Almendro, V., Gascón, P., Bragado, P., & Mancino, M.
731 (2018). Histamine receptor 1 inhibition enhances antitumor therapeutic responses through
732 extracellular signal-regulated kinase (ERK) activation in breast cancer. *Cancer Letters*, *424*, 70-
733 83. https://doi.org/https://doi.org/10.1016/j.canlet.2018.03.014
734 Gabay, M., Li, Y., & Felsher, D. W. (2014). MYC activation is a hallmark of cancer initiation and
735 maintenance. *Cold Spring Harb Perspect Med*, *4*(6).
736 https://doi.org/10.1101/cshperspect.a014241
737 Gelibter, S., Marostica, G., Mandelli, A., Siciliani, S., Podini, P., Finardi, A., & Furlan, R. (2022). The impact
738 of storage on extracellular vesicles: A systematic study. *J Extracell Vesicles*, *11*(2), e12162.
739 https://doi.org/10.1002/jev2.12162
740 Good, P. I. (2006). *Resampling methods: A practical guide to data analysis.* Birkhauser.
741 Görgens, A., Corso, G., Hagey, D. W., Jawad Wiklander, R., Gustafsson, M. O., Felldin, U., Lee, Y.,
742 Bostancioglu, R. B., Sork, H., Liang, X., Zheng, W., Mohammad, D. K., van de Wakker, S. I., Vader,
743 P., Zickler, A. M., Mamand, D. R., Ma, L., Holme, M. N., Stevens, M. M., . . . El Andaloussi, S.
744 (2022). Identification of storage conditions stabilizing extracellular vesicles preparations. *J*
745 *Extracell Vesicles*, *11*(6), e12238. https://doi.org/10.1002/jev2.12238
746 Hatipoglu, O. F., Nishinaka, T., Nishibori, M., Watanabe, M., Toyomura, T., Mori, S., Yaykasli, K. O., Wake,
747 H., & Takahashi, H. (2023). Histamine promotes angiogenesis through a histamine H1 receptor-
748 PKC-VEGF-mediated pathway in human endothelial cells. *Journal of Pharmacological Sciences*,
749 *151*(4), 177-186. https://doi.org/https://doi.org/10.1016/j.jphs.2023.02.006
750 Heydenreich, F. M., Marti-Solano, M., Sandhu, M., Kobilka, B. K., Bouvier, M., & Babu, M. M. (2023).
751 Molecular determinants of ligand efficacy and potency in GPCR signaling. *Science*, *382*(6677),
752 eadh1859. https://doi.org/10.1126/science.adh1859
753 Im, E.-J., Lee, C.-H., Moon, P.-G., Rangaswamy, G. G., Lee, B., Lee, J. M., Lee, J.-C., Jee, J.-G., Bae, J.-S.,
754 Kwon, T.-K., Kang, K.-W., Jeong, M.-S., Lee, J.-E., Jung, H.-S., Ro, H.-J., Jun, S., Kang, W., Seo, S.-Y.,
755 Cho, Y.-E., . . . Baek, M.-C. (2019). Sulfisoxazole inhibits the secretion of small extracellular
756 vesicles by targeting the endothelin receptor A. *Nature Communications*, *10*(1), 1387.
757 https://doi.org/10.1038/s41467-019-09387-4
758 Jin, Y., Ma, L., Zhang, W., Yang, W., Feng, Q., & Wang, H. (2022). Extracellular signals regulate the
759 biogenesis of extracellular vesicles. *Biol Res*, *55*(1), 35. https://doi.org/10.1186/s40659-022-
760 00405-2
761 Kahn, R., Mossberg, M., Ståhl, A. L., Johansson, K., Lopatko Lindman, I., Heijl, C., Segelmark, M.,
762 Mörgelin, M., Leeb-Lundberg, L. M., & Karpman, D. (2017). Microvesicle transfer of kinin B1-
763 receptors is a novel inflammatory mechanism in vasculitis. *Kidney Int*, *91*(1), 96-105.
764 https://doi.org/10.1016/j.kint.2016.09.023
765 Karlsson, M., Zhang, C., Méar, L., Zhong, W., Digre, A., Katona, B., Sjöstedt, E., Butler, L., Odeberg, J.,
766 Dusart, P., Edfors, F., Oksvold, P., von Feilitzen, K., Zwahlen, M., Arif, M., Altay, O., Li, X., Ozcan,
767 M., Mardinoglu, A., . . . Lindskog, C. (2021). A single-cell type transcriptomics map of human
768 tissues. *Sci Adv*, *7*(31). https://doi.org/10.1126/sciadv.abh2169
769 Kim, M. E., Kim, D. H., & Lee, J. S. (2022). FoxO Transcription Factors: Applicability as a Novel Immune
770 Cell Regulators and Therapeutic Targets in Oxidative Stress-Related Diseases. *Int J Mol Sci*,
771 *23*(19). https://doi.org/10.3390/ijms231911877
772 Kozielewicz, P., Shekhani, R., Moser, S., Bowin, C.-F., Wesslowski, J., Davidson, G., & Schulte, G. (2021).
773 Quantitative Profiling of WNT-3A Binding to All Human Frizzled Paralogues in HEK293 Cells by
774 NanoBiT/BRET Assessments. *ACS Pharmacology & Translational Science*, *4*(3), 1235-1245.
775 https://doi.org/10.1021/acsptsci.1c00084

776 Kriebel, P. W., Majumdar, R., Jenkins, L. M., Senoo, H., Wang, W., Ammu, S., Chen, S., Narayan, K., Iijima,
777 M., & Parent, C. A. (2018). Extracellular vesicles direct migration by synthesizing and releasing
778 chemotactic signals. *J Cell Biol*, *217*(8), 2891-2910. https://doi.org/10.1083/jcb.201710170
779 Kritsilis, M., S, V. R., Koutsoudaki, P. N., Evangelou, K., Gorgoulis, V. G., & Papadopoulos, D. (2018).
780 Ageing, Cellular Senescence and Neurodegenerative Disease. *Int J Mol Sci*, *19*(10).
781 https://doi.org/10.3390/ijms19102937
782 Kugeratski, F. G., Hodge, K., Lilla, S., McAndrews, K. M., Zhou, X., Hwang, R. F., Zanivan, S., & Kalluri, R.
783 (2021). Quantitative proteomics identifies the core proteome of exosomes with syntenin-1 as
784 the highest abundant protein and a putative universal biomarker. *Nat Cell Biol*, *23*(6), 631-641.
785 https://doi.org/10.1038/s41556-021-00693-y
786 Lam, E. W. F., Brosens, J. J., Gomes, A. R., & Koo, C.-Y. (2013). Forkhead box proteins: tuning forks for
787 transcriptional harmony. *Nature Reviews Cancer*, *13*(7), 482-495.
788 https://doi.org/10.1038/nrc3539
789 Lee, Y. J., Shin, K. J., Jang, H. J., Ryu, J. S., Lee, C. Y., Yoon, J. H., Seo, J. K., Park, S., Lee, S., Je, A. R., Huh, Y.
790 H., Kong, S. Y., Kwon, T., Suh, P. G., & Chae, Y. C. (2023). GPR143 controls ESCRT-dependent
791 exosome biogenesis and promotes cancer metastasis. *Dev Cell*, *58*(4), 320-334.e328.
792 https://doi.org/10.1016/j.devcel.2023.01.006
793 Lehrich, B. M., Liang, Y., & Fiandaca, M. S. (2021). Foetal bovine serum influence on in vitro extracellular
794 vesicle analyses. *J Extracell Vesicles*, *10*(3), e12061. https://doi.org/10.1002/jev2.12061
795 Li, H., Xiao, Y., Li, Q., Yao, J., Yuan, X., Zhang, Y., Yin, X., Saito, Y., Fan, H., Li, P., Kuo, W. L., Halpin, A.,
796 Gibbons, D. L., Yagita, H., Zhao, Z., Pang, D., Ren, G., Yee, C., Lee, J. J., & Yu, D. (2022). The allergy
797 mediator histamine confers resistance to immunotherapy in cancer patients via activation of the
798 macrophage histamine receptor H1. *Cancer Cell*, *40*(1), 36-52.e39.
799 https://doi.org/10.1016/j.ccell.2021.11.002
800 Li, Y. Z., Di Cristofano, A., & Woo, M. (2020). Metabolic Role of PTEN in Insulin Signaling and Resistance.
801 *Cold Spring Harb Perspect Med*, *10*(8). https://doi.org/10.1101/cshperspect.a036137
802 Liu, Y., Hu, N., Ai, B., Xia, H., & Li, W. (2024). MiR-31-5p alleviates septic cardiomyopathy by targeting
803 BAP1 to inhibit SLC7A11 deubiquitination and ferroptosis. *BMC Cardiovascular Disorders*, *24*(1),
804 286. https://doi.org/10.1186/s12872-024-03954-4
805 Liu, Y., Xu, Z., Zheng, H., Yang, J., Wu, M., Yang, Q., Wang, Y., Zong, T., Yang, X., Xie, T., Cai, J., Yao, Y., &
806 Wang, X. (2023). MiR-423-5p promotes Müller cell activation via targeting NGF signaling in
807 diabetic retinopathy. *Life Sci*, *334*, 122217. https://doi.org/10.1016/j.lfs.2023.122217
808 Mack, M., Kleinschmidt, A., Brühl, H., Klier, C., Nelson, P. J., Cihak, J., Plachý, J., Stangassinger, M., Erfle,
809 V., & Schlöndorff, D. (2000). Transfer of the chemokine receptor CCR5 between cells by
810 membrane-derived microparticles: a mechanism for cellular human immunodeficiency virus 1
811 infection. *Nat Med*, *6*(7), 769-775. https://doi.org/10.1038/77498
812 Majumder, M., Landman, E., Liu, L., Hess, D., & Lala, P. K. (2015). COX-2 Elevates Oncogenic miR-526b in
813 Breast Cancer by EP4 Activation. *Mol Cancer Res*, *13*(6), 1022-1033.
814 https://doi.org/10.1158/1541-7786.Mcr-14-0543
815 Mann, H. B., & Whitney, D. R. (1947). On a test of whether one of two random variables is stochastically
816 larger than the other. *The annals of mathematical statistics*, 50-60.
817 Matthews, H. K., Bertoli, C., & de Bruin, R. A. M. (2022). Cell cycle control in cancer. *Nature Reviews*
818 *Molecular Cell Biology*, *23*(1), 74-88. https://doi.org/10.1038/s41580-021-00404-3
819 Mazzeo, C., Calvo, V., Alonso, R., Mérida, I., & Izquierdo, M. (2016). Protein kinase D1/2 is involved in
820 the maturation of multivesicular bodies and secretion of exosomes in T and B lymphocytes. *Cell*
821 *Death & Differentiation*, *23*(1), 99-109. https://doi.org/10.1038/cdd.2015.72
822 Montastier, E., Beuzelin, D., Martins, F., Mir, L., Marqués, M. A., Thalamas, C., Iacovoni, J., Langin, D., &
823 Viguerie, N. (2019). Niacin induces miR-502-3p expression which impairs insulin sensitivity in

824 human adipocytes. *Int J Obes (Lond)*, *43*(7), 1485-1490. https://doi.org/10.1038/s41366-018-
825 0260-5
826 Németh, A., Orgovan, N., Sódar, B. W., Osteikoetxea, X., Pálóczi, K., Szabó-Taylor, K. É., Vukman, K. V.,
827 Kittel, Á., Turiák, L., Wiener, Z., Tóth, S., Drahos, L., Vékey, K., Horvath, R., & Buzás, E. I. (2017).
828 Antibiotic-induced release of small extracellular vesicles (exosomes) with surface-associated
829 DNA. *Sci Rep*, *7*(1), 8202. https://doi.org/10.1038/s41598-017-08392-1
830 Nordin, J. Z. (2022). Transfection reagents affect Extracellular Vesicle cargo transfer to recipient cells:
831 The importance of appropriate controls in EV research. *J Extracell Vesicles*, *11*(10), e12227.
832 https://doi.org/10.1002/jev2.12227
833 Odegaard, K. E., Chand, S., Wheeler, S., Tiwari, S., Flores, A., Hernandez, J., Savine, M., Gowen, A.,
834 Pendyala, G., & Yelamanchili, S. V. (2020). Role of Extracellular Vesicles in Substance Abuse and
835 HIV-Related Neurological Pathologies. *Int J Mol Sci*, *21*(18).
836 https://doi.org/10.3390/ijms21186765
837 Ofer, D., & Linial, M. (2022). Inferring microRNA regulation: A proteome perspective. *Front Mol Biosci*, *9*,
838 916639. https://doi.org/10.3389/fmolb.2022.916639
839 Oliner, J. D., Saiki, A. Y., & Caenepeel, S. (2016). The Role of MDM2 Amplification and Overexpression in
840 Tumorigenesis. *Cold Spring Harb Perspect Med*, *6*(6).
841 https://doi.org/10.1101/cshperspect.a026336
842 Orr-Burks, N., Murray, J., Todd, K. V., Bakre, A., & Tripp, R. A. (2021). MicroRNAs affect GPCR and Ion
843 channel genes needed for influenza replication. *J Gen Virol*, *102*(11).
844 https://doi.org/10.1099/jgv.0.001691
845 Ortega, F. J., Mercader, J. M., Catalán, V., Moreno-Navarrete, J. M., Pueyo, N., Sabater, M., Gómez-
846 Ambrosi, J., Anglada, R., Fernández-Formoso, J. A., Ricart, W., Frühbeck, G., & Fernández-Real, J.
847 M. (2013). Targeting the circulating microRNA signature of obesity. *Clin Chem*, *59*(5), 781-792.
848 https://doi.org/10.1373/clinchem.2012.195776
849 Palmisano, G., Jensen, S. S., Le Bihan, M. C., Lainé, J., McGuire, J. N., Pociot, F., & Larsen, M. R. (2012).
850 Characterization of membrane-shed microvesicles from cytokine-stimulated β-cells using
851 proteomics strategies. *Mol Cell Proteomics*, *11*(8), 230-243.
852 https://doi.org/10.1074/mcp.M111.012732
853 Palumbo, M. C., Gautam, M., Sonneborn, A., Kim, K., Wilmarth, P. A., Reddy, A. P., Shi, X., Marks, D. L.,
854 Sahay, G., Abbas, A. I., & Janowsky, A. (2023). MicroRNA137-loaded lipid nanoparticles regulate
855 synaptic proteins in the prefrontal cortex. *Molecular Therapy*, *31*(10), 2975-2990.
856 https://doi.org/https://doi.org/10.1016/j.ymthe.2023.08.016
857 Palviainen, M., Saari, H., Kärkkäinen, O., Pekkinen, J., Auriola, S., Yliperttula, M., Puhka, M., Hanhineva,
858 K., & Siljander, P. R. (2019). Metabolic signature of extracellular vesicles depends on the cell
859 culture conditions. *J Extracell Vesicles*, *8*(1), 1596669.
860 https://doi.org/10.1080/20013078.2019.1596669
861 Papadopoulos, D., Magliozzi, R., Mitsikostas, D. D., Gorgoulis, V. G., & Nicholas, R. S. (2020). Aging,
862 Cellular Senescence, and Progressive Multiple Sclerosis. *Front Cell Neurosci*, *14*, 178.
863 https://doi.org/10.3389/fncel.2020.00178
864 Park, C., Lee, J. W., Kim, K., Seen, D. S., Jeong, J. Y., & Huh, W. K. (2023). Simultaneous activation of CXC
865 chemokine receptor 4 and histamine receptor H1 enhances calcium signaling and cancer cell
866 migration. *Sci Rep*, *13*(1), 1894. https://doi.org/10.1038/s41598-023-28531-1
867 Patel, S., Doble, B. W., MacAulay, K., Sinclair, E. M., Drucker, D. J., & Woodgett, J. R. (2008). Tissue-
868 specific role of glycogen synthase kinase 3beta in glucose homeostasis and insulin action. *Mol
869 Cell Biol*, *28*(20), 6314-6328. https://doi.org/10.1128/mcb.00763-08

870 Perez-Vilar, J., & Hill, R. L. (1997). Norrie Disease Protein (Norrin) Forms Disulfide-linked Oligomers
871 Associated with the Extracellular Matrix*. *Journal of Biological Chemistry*, *272*(52), 33410-
872 33415. https://doi.org/https://doi.org/10.1074/jbc.272.52.33410
873 Pfeffer, C. M., & Singh, A. T. K. (2018). Apoptosis: A Target for Anticancer Therapy. *Int J Mol Sci*, *19*(2).
874 https://doi.org/10.3390/ijms19020448
875 Pham, C. V., Midge, S., Barua, H., Zhang, Y., Ngoc-Gia Nguyen, T., Barrero, R. A., Duan, A., Yin, W., Jiang,
876 G., Hou, Y., Zhou, S., Wang, Y., Xie, X., Tran, P. H. L., Xiang, D., & Duan, W. (2021). Bovine
877 extracellular vesicles contaminate human extracellular vesicles produced in cell culture
878 conditioned medium when 'exosome-depleted serum' is utilised. *Archives of Biochemistry and*
879 *Biophysics*, *708*, 108963. https://doi.org/https://doi.org/10.1016/j.abb.2021.108963
880 Plotnikova, O., Baranova, A., & Skoblov, M. (2019). Comprehensive Analysis of Human microRNA-mRNA
881 Interactome. *Front Genet*, *10*, 933. https://doi.org/10.3389/fgene.2019.00933
882 Reichelt, M. E., Willems, L., Molina, J. G., Sun, C. X., Noble, J. C., Ashton, K. J., Schnermann, J., Blackburn,
883 M. R., & Headrick, J. P. (2005). Genetic deletion of the A1 adenosine receptor limits myocardial
884 ischemic tolerance. *Circ Res*, *96*(3), 363-367.
885 https://doi.org/10.1161/01.Res.0000156075.00127.C3
886 Ripke, S., Neale, B. M., Corvin, A., Walters, J. T. R., Farh, K.-H., Holmans, P. A., Lee, P., Bulik-Sullivan, B.,
887 Collier, D. A., Huang, H., Pers, T. H., Agartz, I., Agerbo, E., Albus, M., Alexander, M., Amin, F.,
888 Bacanu, S. A., Begemann, M., Belliveau Jr, R. A., . . . Psychosis Endophenotypes International, C.
889 (2014). Biological insights from 108 schizophrenia-associated genetic loci. *Nature*, *511*(7510),
890 421-427. https://doi.org/10.1038/nature13595
891 Rothman, J. E. (1996). The protein machinery of vesicle budding and fusion. *Protein Sci*, *5*(2), 185-194.
892 https://doi.org/10.1002/pro.5560050201
893 Ryzhov, S., Matafonov, A., Galindo, C. L., Zhang, Q., Tran, T. L., Lenihan, D. J., Lenneman, C. G.,
894 Feoktistov, I., & Sawyer, D. B. (2017). ERBB signaling attenuates proinflammatory activation of
895 nonclassical monocytes. *Am J Physiol Heart Circ Physiol*, *312*(5), H907-h918.
896 https://doi.org/10.1152/ajpheart.00486.2016
897 Sandau, U. S., Duggan, E., Shi, X., Smith, S. J., Huckans, M., Schutzer, W. E., Loftis, J. M., Janowsky, A.,
898 Nolan, J. P., & Saugstad, J. A. (2020). Methamphetamine use alters human plasma extracellular
899 vesicles and their microRNA cargo: An exploratory study. *J Extracell Vesicles*, *10*(1), e12028.
900 https://doi.org/10.1002/jev2.12028
901 Sandau, U. S., McFarland, T. J., Smith, S. J., Galasko, D. R., Quinn, J. F., & Saugstad, J. A. (2022).
902 Differential Effects of APOE Genotype on MicroRNA Cargo of Cerebrospinal Fluid Extracellular
903 Vesicles in Females With Alzheimer's Disease Compared to Males. *Front Cell Dev Biol*, *10*,
904 864022. https://doi.org/10.3389/fcell.2022.864022
905 Shi, Z., Fultz, R. S., Engevik, M. A., Gao, C., Hall, A., Major, A., Mori-Akiyama, Y., & Versalovic, J. (2019).
906 Distinct roles of histamine H1- and H2-receptor signaling pathways in inflammation-associated
907 colonic tumorigenesis. *Am J Physiol Gastrointest Liver Physiol*, *316*(1), G205-g216.
908 https://doi.org/10.1152/ajpgi.00212.2018
909 Sidhom, K., Obi, P. O., & Saleem, A. (2020). A Review of Exosomal Isolation Methods: Is Size Exclusion
910 Chromatography the Best Option? *Int J Mol Sci*, *21*(18). https://doi.org/10.3390/ijms21186466
911 Sigismund, S., Avanzato, D., & Lanzetti, L. (2018). Emerging functions of the EGFR in cancer. *Mol Oncol*,
912 *12*(1), 3-20. https://doi.org/10.1002/1878-0261.12155
913 Skillings, J. H., & Mack, G. A. (1981). On the use of a Friedman-type statistic in balanced and unbalanced
914 block designs. *Technometrics*, *23*(2), 171-177.
915 Sriram, K., & Insel, P. A. (2018). G Protein-Coupled Receptors as Targets for Approved Drugs: How Many
916 Targets and How Many Drugs? *Mol Pharmacol*, *93*(4), 251-258.
917 https://doi.org/10.1124/mol.117.111062

Stevens, R. C., Cherezov, V., Katritch, V., Abagyan, R., Kuhn, P., Rosen, H., & Wüthrich, K. (2013). The GPCR Network: a large-scale collaboration to determine human GPCR structure and function. *Nat Rev Drug Discov*, *12*(1), 25-34. https://doi.org/10.1038/nrd3859

Strakova, K., Matricon, P., Yokota, C., Arthofer, E., Bernatik, O., Rodriguez, D., Arenas, E., Carlsson, J., Bryja, V., & Schulte, G. (2017). The tyrosine Y250(2.39) in Frizzled 4 defines a conserved motif important for structural integrity of the receptor and recruitment of Disheveled. *Cell Signal*, *38*, 85-96. https://doi.org/10.1016/j.cellsig.2017.06.018

Suelves, N., Saleki, S., Ibrahim, T., Palomares, D., Moonen, S., Koper, M. J., Vrancx, C., Vadukul, D. M., Papadopoulos, N., Viceconte, N., Claude, E., Vandenberghe, R., von Arnim, C. A. F., Constantinescu, S. N., Thal, D. R., Decottignies, A., & Kienlen-Campard, P. (2023). Senescence-related impairment of autophagy induces toxic intraneuronal amyloid-β accumulation in a mouse model of amyloid pathology. *Acta Neuropathol Commun*, *11*(1), 82. https://doi.org/10.1186/s40478-023-01578-x

Tabara, H., Yigit, E., Siomi, H., & Mello, C. C. (2002). The dsRNA binding protein RDE-4 interacts with RDE-1, DCR-1, and a DExH-box helicase to direct RNAi in C. elegans. *Cell*, *109*(7), 861-871. https://doi.org/10.1016/s0092-8674(02)00793-6

Tao, S., He, H., & Chen, Q. (2015). Estradiol induces HOTAIR levels via GPER-mediated miR-148a inhibition in breast cancer. *J Transl Med*, *13*, 131. https://doi.org/10.1186/s12967-015-0489-x

Tetta, C., Ghigo, E., Silengo, L., Deregibus, M. C., & Camussi, G. (2013). Extracellular vesicles as an emerging mechanism of cell-to-cell communication. *Endocrine*, *44*(1), 11-19. https://doi.org/10.1007/s12020-012-9839-0

Verweij, F. J., Bebelman, M. P., Jimenez, C. R., Garcia-Vallejo, J. J., Janssen, H., Neefjes, J., Knol, J. C., De Goeij-De Haas, R., Piersma, S. R., Baglio, S. R., Verhage, M., Middeldorp, J. M., Zomer, A., Van Rheenen, J., Coppolino, M. G., Hurbain, I., Raposo, G., Smit, M. J., Toonen, R. F. G., . . . Pegtel, D. M. (2018). Quantifying exosome secretion from single cells reveals a modulatory role for GPCR signaling. *Journal of Cell Biology*, *217*(3), 1129-1142. https://doi.org/10.1083/jcb.201703206

Verweij, F. J., Bebelman, M. P., Jimenez, C. R., Garcia-Vallejo, J. J., Janssen, H., Neefjes, J., Knol, J. C., de Goeij-de Haas, R., Piersma, S. R., Baglio, S. R., Verhage, M., Middeldorp, J. M., Zomer, A., van Rheenen, J., Coppolino, M. G., Hurbain, I., Raposo, G., Smit, M. J., Toonen, R. F. G., . . . Pegtel, D. M. (2018). Quantifying exosome secretion from single cells reveals a modulatory role for GPCR signaling. *J Cell Biol*, *217*(3), 1129-1142. https://doi.org/10.1083/jcb.201703206

Wang, H. L., Wei, B., He, H. J., Huang, X. R., Sheng, J. Y., Chen, X. C., Wang, L., Tan, R. Z., Li, J. C., Liu, J., Yang, S. J., Ma, R. C., & Lan, H. Y. (2022). Smad3 deficiency improves islet-based therapy for diabetes and diabetic kidney injury by promoting β cell proliferation via the E2F3-dependent mechanism. *Theranostics*, *12*(1), 379-395. https://doi.org/10.7150/thno.67034

Wang, K. Y., Tanimoto, A., Yamada, S., Guo, X., Ding, Y., Watanabe, T., Watanabe, T., Kohno, K., Hirano, K., Tsukada, H., & Sasaguri, Y. (2010). Histamine regulation in glucose and lipid metabolism via histamine receptors: model for nonalcoholic steatohepatitis in mice. *Am J Pathol*, *177*(2), 713-723. https://doi.org/10.2353/ajpath.2010.091198

Wang, Q., Bode, A. M., & Zhang, T. (2023). Targeting CDK1 in cancer: mechanisms and implications. *npj Precision Oncology*, *7*(1), 58. https://doi.org/10.1038/s41698-023-00407-7

Wang, Y., Pan, W., Bai, X., Wang, X., Wang, Y., & Yin, Y. (2021). microRNA-454-mediated NEDD4-2/TrkA/cAMP axis in heart failure: Mechanisms and cardioprotective implications. *J Cell Mol Med*, *25*(11), 5082-5098. https://doi.org/10.1111/jcmm.16491

Wang, Z., Wu, L., Wang, H., Zhang, Y., & Xiao, H. (2022). Agonist-induced extracellular vesicles contribute to the transfer of functional bombesin receptor-subtype 3 to recipient cells. *Cellular and Molecular Life Sciences*, *79*(1). https://doi.org/10.1007/s00018-021-04114-z

965 Watts, V. J., Wiens, B. L., Cumbay, M. G., Vu, M. N., Neve, R. L., & Neve, K. A. (1998). Selective activation
966 of Galphao by D2L dopamine receptors in NS20Y neuroblastoma cells. *J Neurosci*, *18*(21), 8692-
967 8699. https://doi.org/10.1523/jneurosci.18-21-08692.1998
968 Welch, B. L. (1947). The generalisation of student's problems when several different population
969 variances are involved. *Biometrika*, *34*(1-2), 28-35. https://doi.org/10.1093/biomet/34.1-2.28
970 Xu, Q., Wang, Y., Dabdoub, A., Smallwood, P. M., Williams, J., Woods, C., Kelley, M. W., Jiang, L., Tasman,
971 W., Zhang, K., & Nathans, J. (2004). Vascular development in the retina and inner ear: control by
972 Norrin and Frizzled-4, a high-affinity ligand-receptor pair. *Cell*, *116*(6), 883-895.
973 https://doi.org/10.1016/s0092-8674(04)00216-8
974 Yang, W., Wang, J., Chen, Z., Chen, J., Meng, Y., Chen, L., Chang, Y., Geng, B., Sun, L., Dou, L., Li, J., Guan,
975 Y., Cui, Q., & Yang, J. (2017). NFE2 Induces miR-423-5p to Promote Gluconeogenesis and
976 Hyperglycemia by Repressing the Hepatic FAM3A-ATP-Akt Pathway. *Diabetes*, *66*(7), 1819-1832.
977 https://doi.org/10.2337/db16-1172
978 Yang, Y. M., Lee, C. G., Koo, J. H., Kim, T. H., Lee, J. M., An, J., Kim, K. M., & Kim, S. G. (2015). Gα12
979 overexpressed in hepatocellular carcinoma reduces microRNA-122 expression via HNF4α
980 inactivation, which causes c-Met induction. *Oncotarget*, *6*(22), 19055-19069.
981 https://doi.org/10.18632/oncotarget.3957
982 Zhang, H., Artiles, K. L., & Fire, A. Z. (2015). Functional relevance of "seed" and "non-seed" sequences in
983 microRNA-mediated promotion of C. elegans developmental progression. *Rna*, *21*(11), 1980-
984 1992. https://doi.org/10.1261/rna.053793.115
985 Zhang, Y., Xing, H., Guo, S., Zheng, Z., Wang, H., & Xu, D. (2016). MicroRNA-135b has a neuroprotective
986 role via targeting of β-site APP-cleaving enzyme 1. *Exp Ther Med*, *12*(2), 809-814.
987 https://doi.org/10.3892/etm.2016.3366
988 Zhang, Z., Lin, X., Wei, L., Wu, Y., Xu, L., Wu, L., Wei, X., Zhao, S., Zhu, X., & Xu, F. (2024). A framework for
989 Frizzled-G protein coupling and implications to the PCP signaling pathways. *Cell Discov*, *10*(1), 3.
990 https://doi.org/10.1038/s41421-023-00627-y
991 Zhao, L., Qian, X., Ren, Z., & Wang, A. (2024). miR-31-5p suppresses myocardial hypertrophy by targeting
992 Nfatc2ip. *J Cell Mol Med*, *28*(12), e18413. https://doi.org/10.1111/jcmm.18413

993

994

995

996

997

998

999

1000

1001

15. FIGURES AND TABLES

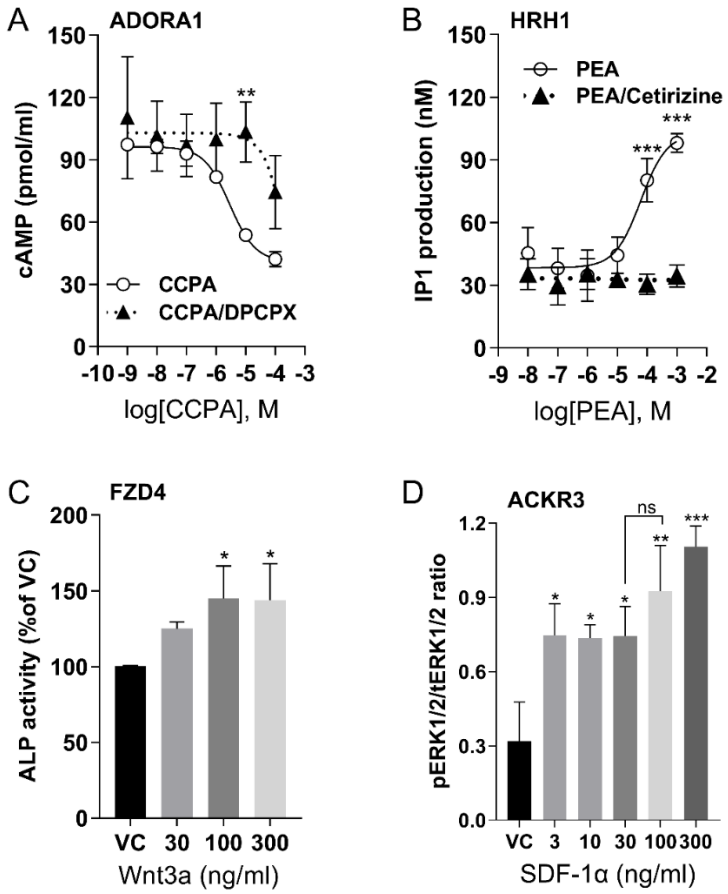

Figure 1. GPCR activation in U2OS cells by selective agonists

(**A**) Dose-dependent cAMP accumulation after ADORA1 activation with agonist, CCPA, or inhibition with antagonist DPCPX (5μM). (**B**) Dose-dependent IP1 accumulation after PEA stimulation of HRH1 and inhibition by Cetirizine (1μM). (**C**) ALP activity after stimulation of FZD4 by Wnt3a. (**D**) The ratio of phosphorylated ERK1/2 (pERK1/2) by total ERK 1/2 (tERK1/2) after stimulation of ACKR3 by SDF-1α. For all graphs, data are shown as mean ± SD, with n=3 independent repeats, each having duplicate determinants, ns=not significant, *$p < 0.05$, **$p < 0.01$, ***$p < 0.001$ vs vehicle control (VC). Statistical significances were determined by one way or two-way ANOVA of receptors by agonists or antagonists and post-hoc Tukey or Sidak testing for multiple comparisons.

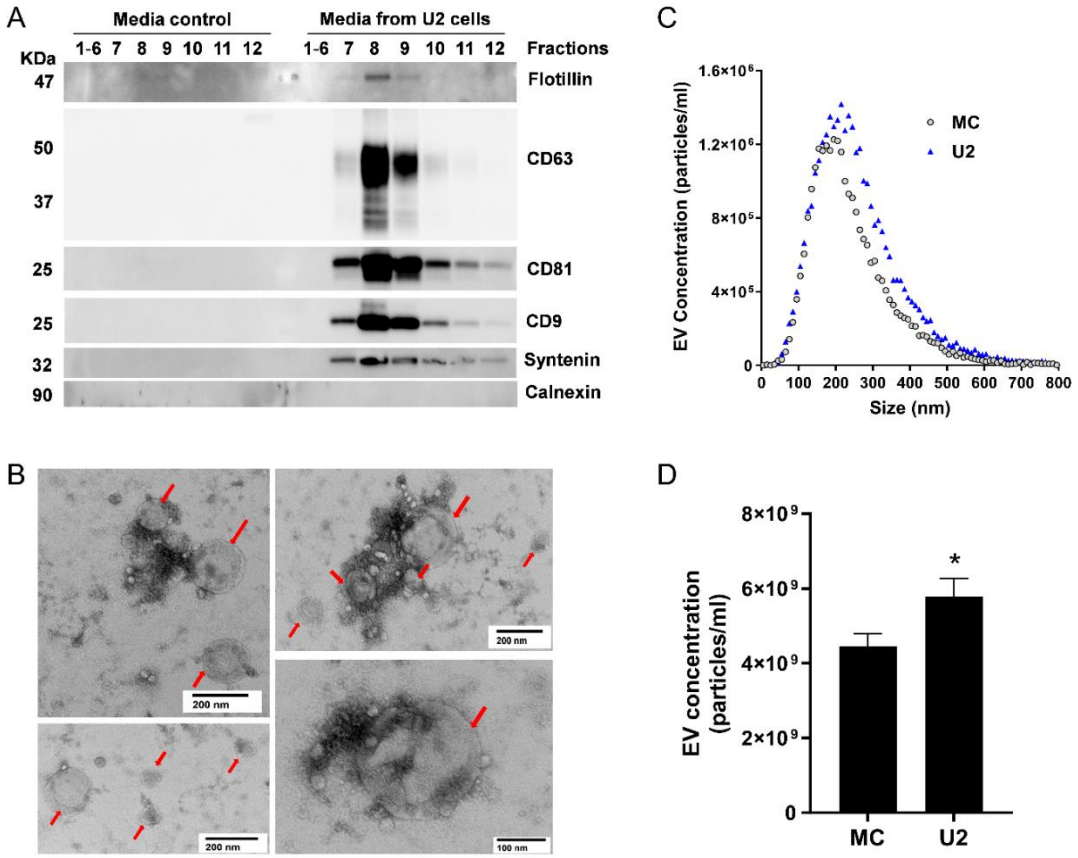

Figure 2. Characterization of EVs isolated from U2OS cell culture media

(**A**) Representative immunoblots of EVs isolated by SEC from U2OS cell culture media (U2) but not from media control (MC) show detection of EV markers including CD9, CD63, CD81, flotillin, and syntenin, in EV fractions 7-9. Endoplasmic reticulum marker, calnexin, was not detected in the EV fractions. (**B**) Representative images from transmission electron microscopy of isolated EVs (red arrows) from pooled EV-enriched fractions 7-9. (**C**) Size distribution of pooled EV fractions 7-9 isolated from MC and U2. (**D**) Quantification of pooled EV fractions 7-9 of MC and U2 measured by f-NTA. Data are shown as mean ± SEM, n=7-8. A Student's *t*-test determined significant differences in the EV concentration between the MC and U2, $*p < 0.05$.

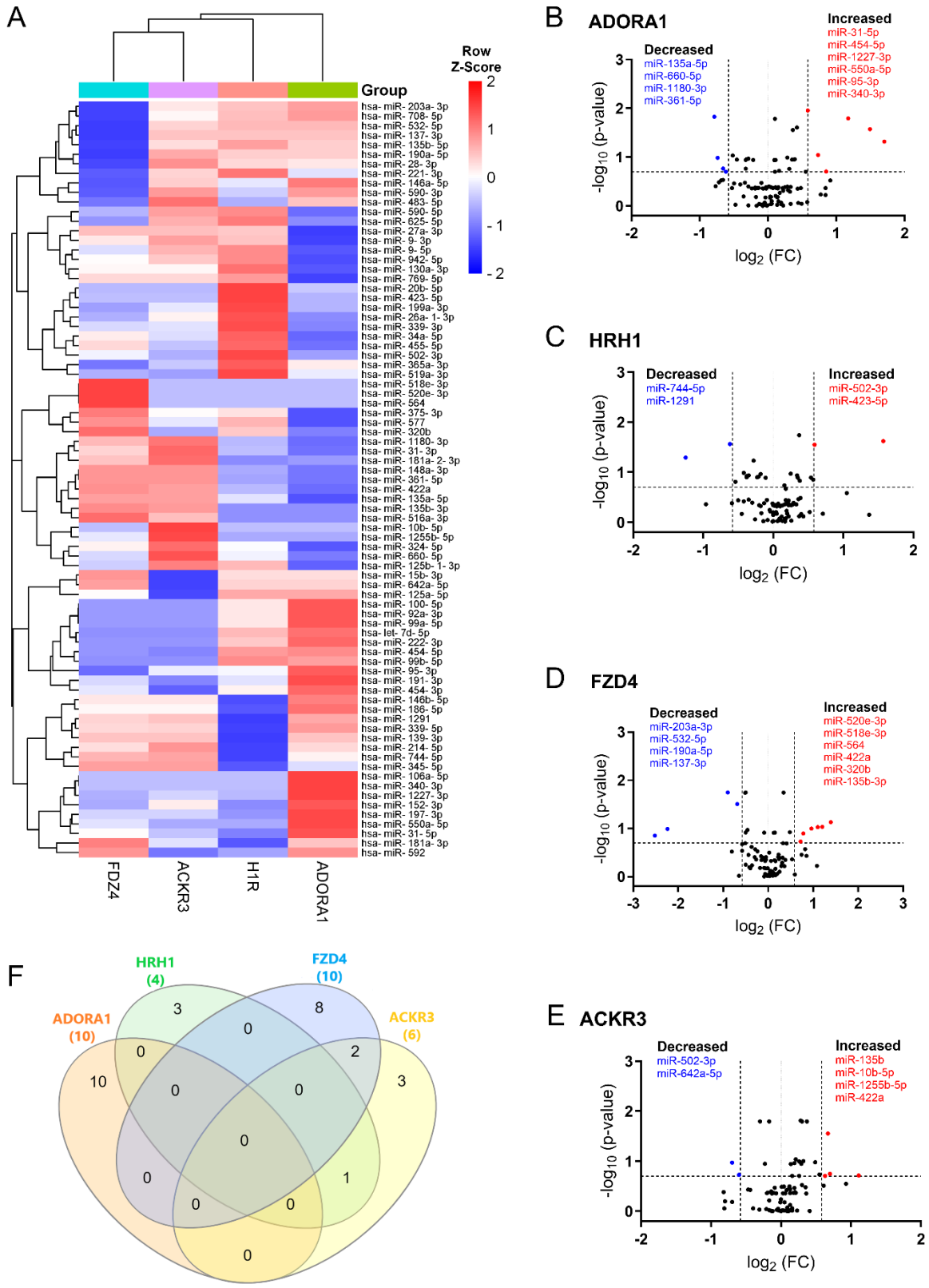
A
Row Z-Score
2
1
0
- 1
- 2
Group
FDZ4
ACKR3
H1R
ADORA1
B
ADORA1
Decreased
miR-135a-5p
miR-660-5p
miR-1180-3p
miR-361-5p
Increased
miR-31-5p
miR-454-5p
miR-1227-3p
miR-550a-5p
miR-95-3p
miR-340-3p
-log10 (p-value)
log2 (FC)
C
HRH1
Decreased
miR-744-5p
miR-1291
Increased
miR-502-3p
miR-423-5p
D
FZD4
Decreased
miR-203a-3p
miR-532-5p
miR-190a-5p
miR-137-3p
Increased
miR-520e-3p
miR-518e-3p
miR-564
miR-422a
miR-320b
miR-135b-3p
E
ACKR3
Decreased
miR-502-3p
miR-642a-5p
Increased
miR-135b
miR-10b-5p
miR-1255b-5p
miR-422a
F
HRH1 (4)
FZD4 (10)
ADORA1 (10)
ACKR3 (6)

1026

Figure 3. Differentially expressed EV miRNAs in response to GPCR activation

(**A**) The heatmap showed unsupervised hierarchical clustering of miRNA expression (row) following GPCR stimulation (column). The relative abundance of miRNAs is represented in Z-score value (z-transformed fold changes), blue, below-mean expression; red, above-mean expression. (**B-E**) Volcano plots displayed the analysis of EV miRNAs after ADORA1 (**B**), HRH1 (**C**), FZD4 (**D**), and ACKR3 (**E**) activation. On the x-axis, the dotted line indicates miRNAs that satisfied the $|\log_2 \text{fold change}| \geq 1.5$ cut-off, while the dotted line on the y-axis indicates miRNA that met Skillings-Mack p-value < 0.2. (**F**) Venn diagram showed the miRNAs of interest with at least 1.5-fold change across four GPCR groups following treatment. n=5-6 replicates per GPCR group.

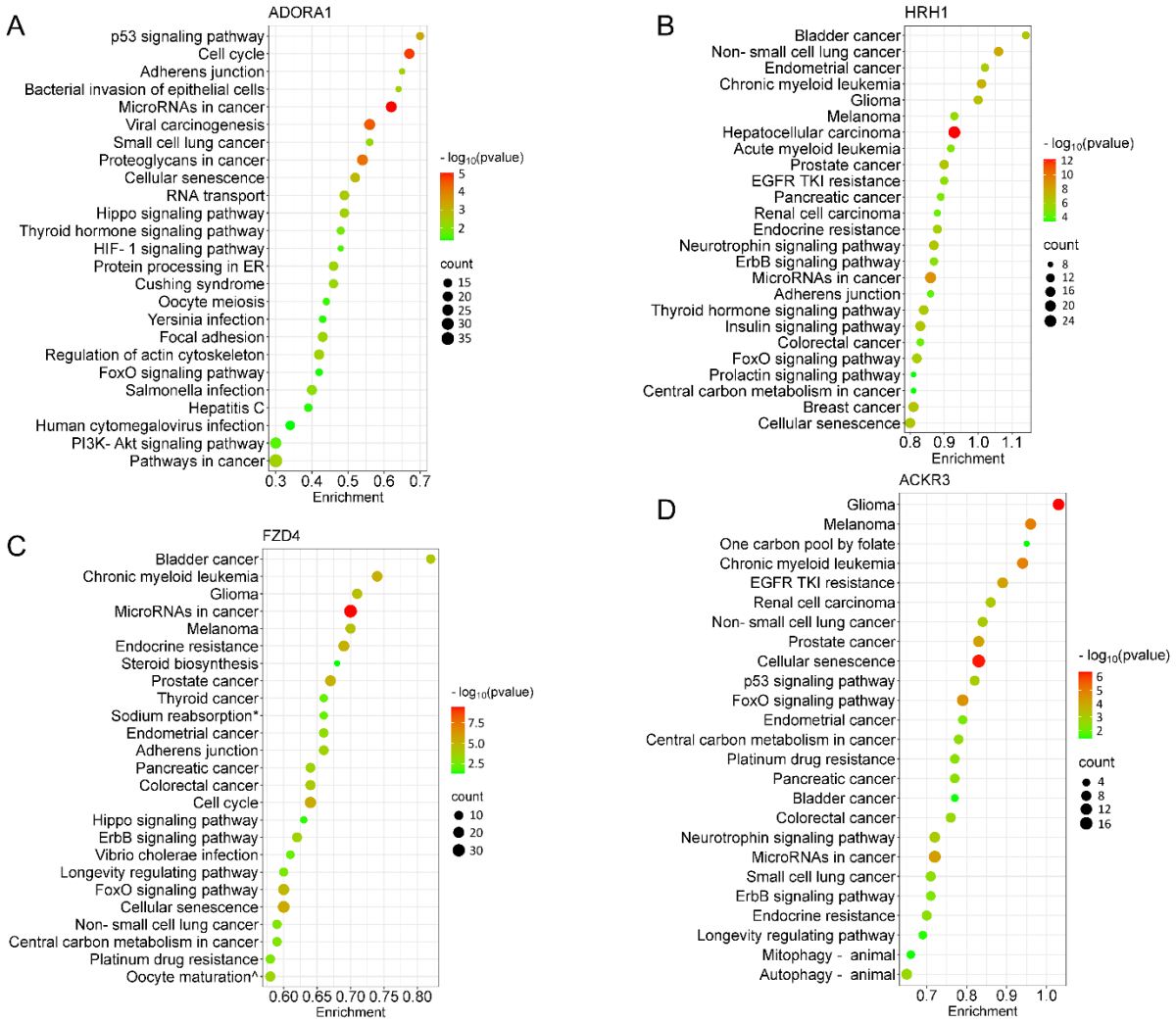

Figure 4. Pathway analysis of the differentially expressed EV miRNA after GPCR activation

The bubble plots showed the top 25 significantly enriched KEGG pathways for the miRNAs (≥ 1.5-fold change) of individual GPCR. (**A**) ADORA1, (**B**) HRH1, (**C**) FZD4, (**D**) ACKR3. The dot size represents the number of enriched gene targets, and the color shows the *p*-value of the enrichment. For the enrichment analysis, cut-off criteria were *p*-value (FDR) < 0.05 and gene count > 2. KEGG terms: * Endocrine and other factor-regulated calcium reabsorption, ^ Progesterone-mediated oocyte maturation.

GPCRs	miRNAs	log_2 (FC)	*p* value	SD of log_2(FC)
ADORA1	hsa-miR-550a-5p	1.70	0.0455	0.22
	hsa-miR-1227-3p	1.49	0.0253	0.16
	hsa-miR-454-5p	1.17	0.0143	0.27
	hsa-miR-31-5p	0.58	0.0143	0.07
	hsa-miR-135a-5p	-0.79	0.0143	0.18
HRH1	hsa-miR-502-3p	1.57	0.025	0.26
	hsa-miR-423-5p	0.59	0.025	0.16
	hsa-miR-744-5p	-0.62	0.025	0.14
FZD4	hsa-miR-203a-3p	-0.90	0.0143	0.16
ACKR3	hsa-miR-135b-3p	0.67	0.0253	0.11

Table 1. EV miRNAs differentially expressed in 4 GPCR groups.

Differentially expressed miRNAs ($p < 0.05$) were identified in each treatment group compared to its vehicle control, n=5-6 samples of each group.